Laser Research Center

International Conference on Applied Physics & Imaging
(ICAPI)
20 - 21 September 2025 | Tartu, Estonia

Vilnius University
Excellence Center of Advanced Light Technologies

Generation of helical intensity beams and pulses for micromachining

Gabrielius Kontenis

Tartu, Estonia
2025-09-21

Laser Research Center

Vilnius University Excellence Center of Advanced Light Technologies

- All topics related to femtosecond micromachining

Metal processing:
- Surface treatment,
- Deep cutting
- Polishing

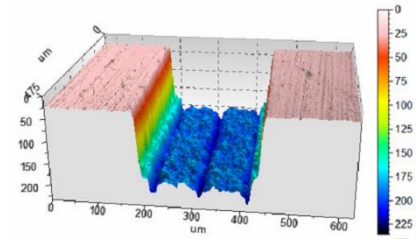

Deep engraving in stainless steel

Optical fiber processing:
- Selective ablation:
- Microdrilling,
- Core modification

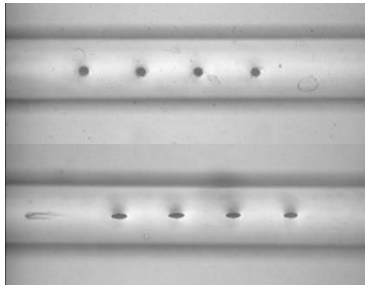

Drilling in optical fibers

Thin coating processing
- Selective ablation
- Laser lift-off of GaN

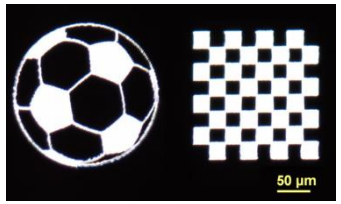

Processing chromium masks for lithography

Laser-assisted chemical etching of dielectrics

- Ultra precision cutting of fused silica
- All-glass MEMS
- Saphire processing

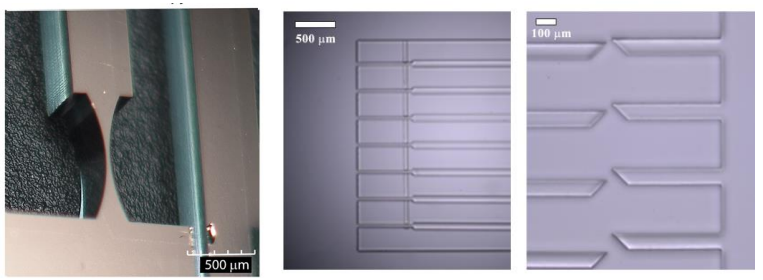

Glass MEMS devices

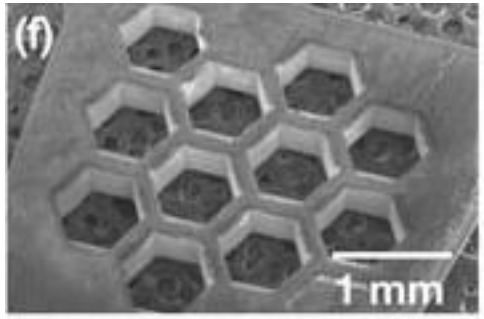

Saphire cutting

For more details feel free to contact **femtosecond micromachining lab**:
dr. Domas Paipulas,
domas.paipulas@ff.vu.lt

Spatial beam shaping and their applications

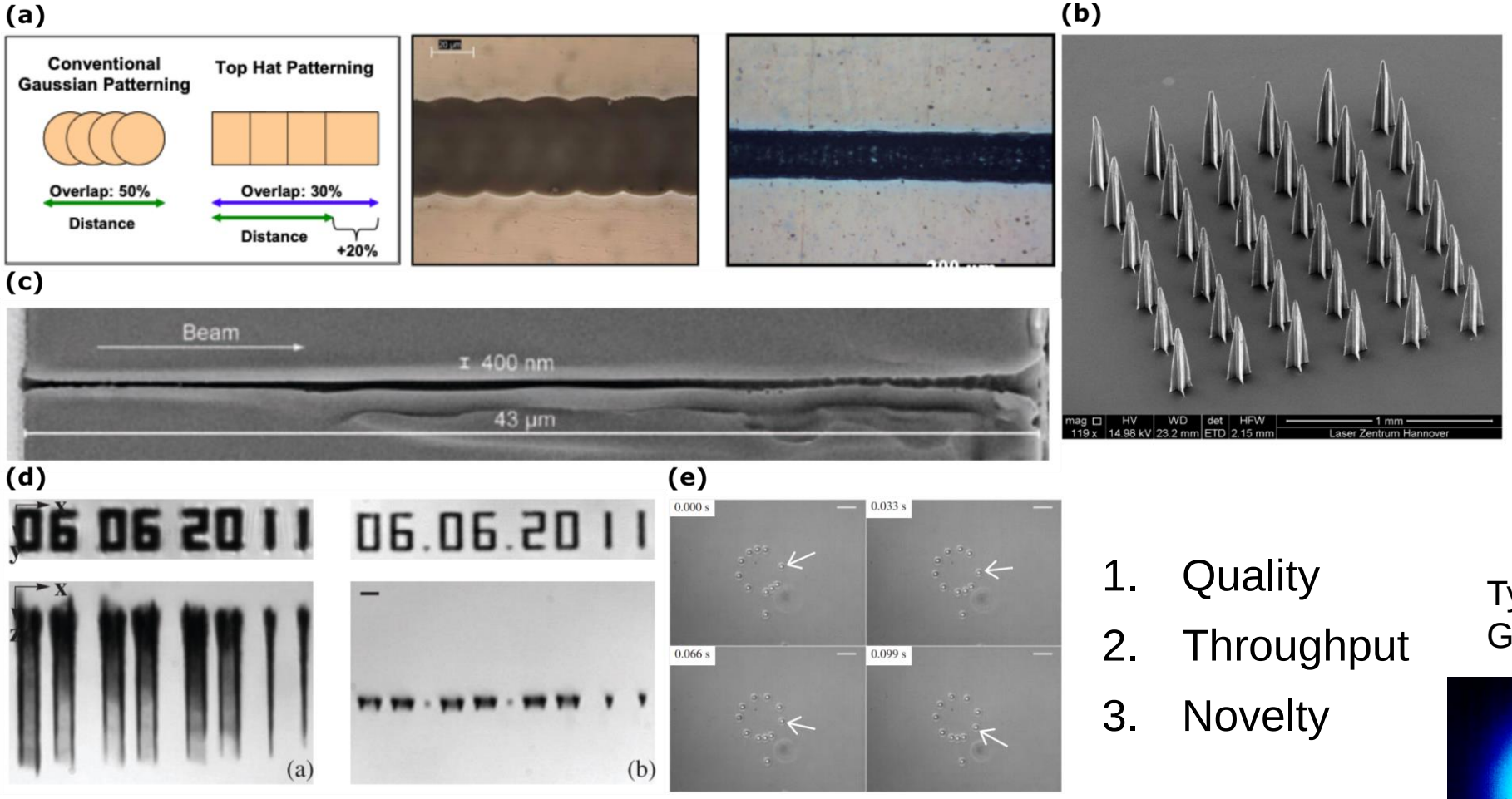

1. Quality
2. Throughput
3. Novelty

Typical initial beam – Gaussian beam

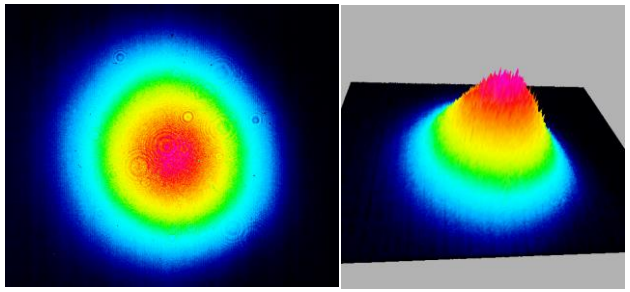

[1] O. Homburg, et al., Proc. of SPIE **8236(**9), (2012)
[2] S.D. Gittard, et al., Biomed. Opt. Express **2**(11), (2011)
[3] M. Duocastella, et al., Laser Photonics Rev. **6**(5), (2012)
[4] R.D. Simmonds, et al., Opt. Express **19**(24), (2011)
[5] V. Garbin, et al., Japanese J. Appl. Physics **44**(7B), (2005)

Expanding the tool set

- Particle manipulation and translational motion with LG beams,
- Stabilization of cold atoms.

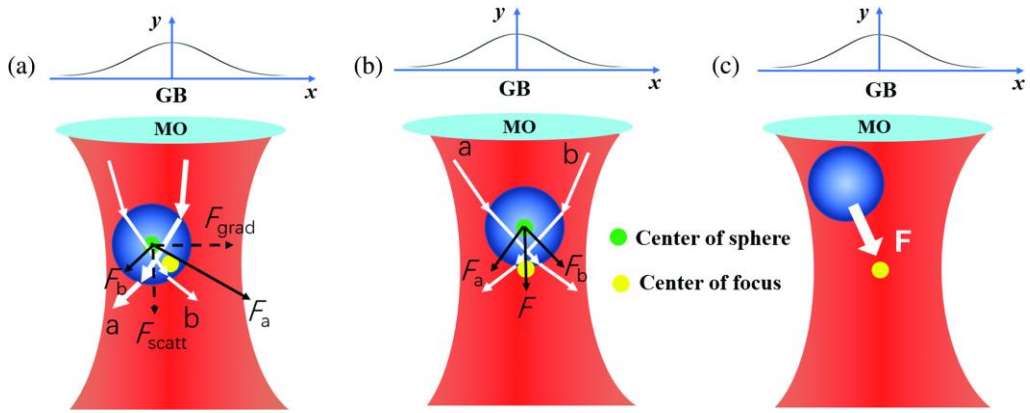

Fig. Working principles of optical tweezers [1].

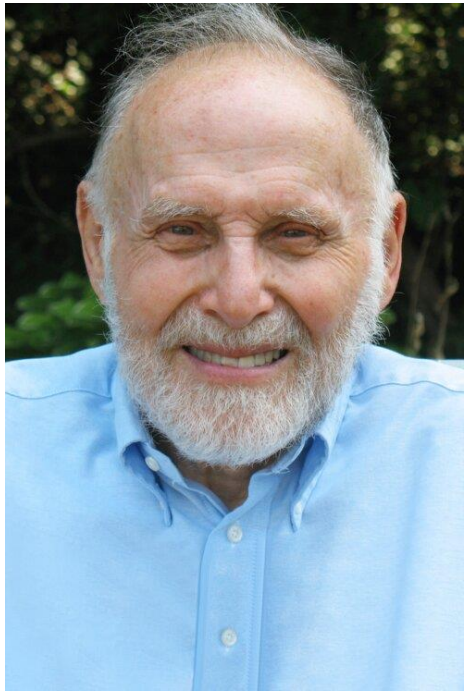

Arthur Ashkin

Nobel Prize in Physics 2018

Mechanical

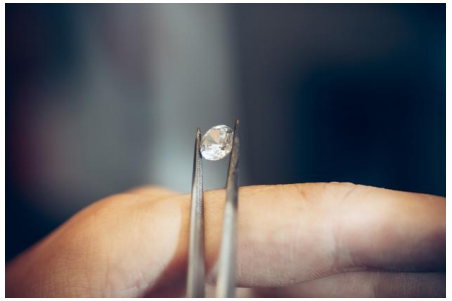

[1] Y. Yuanjie, et al., Advanced Photonics **3**(3), (2021)

Formation of higher order beams

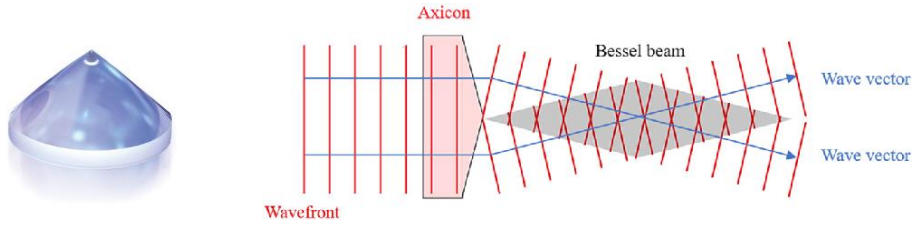

Fig. Working principles of an axicon [1].

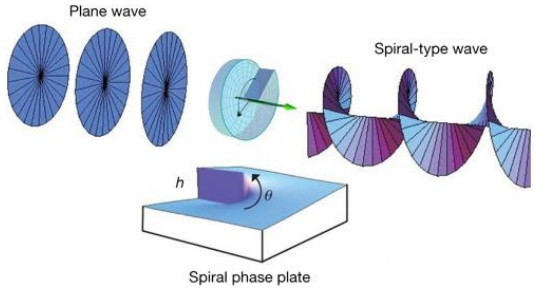

Fig. Working principles of a spiral phase plate for creating an optical vortex [2].

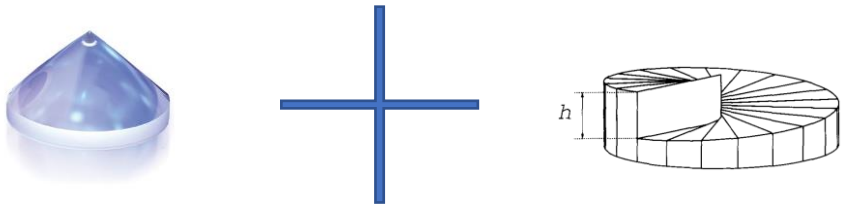

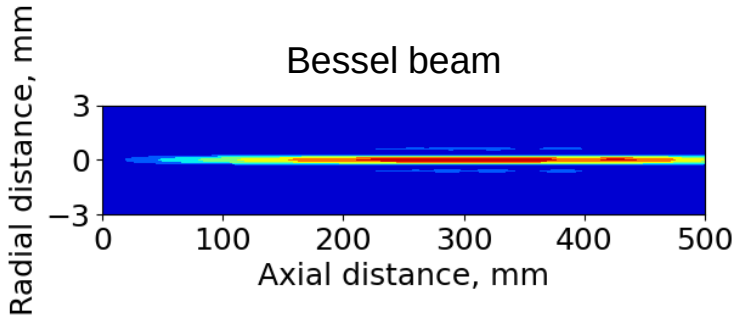

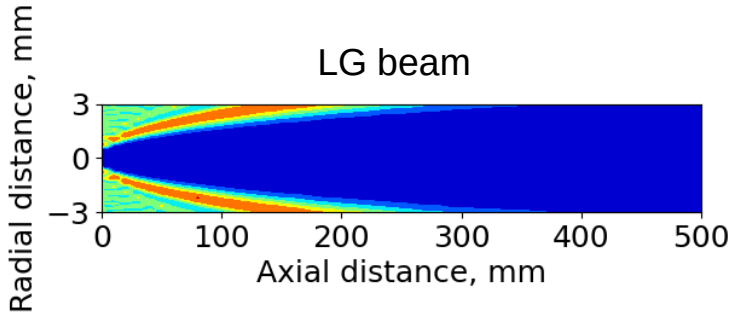

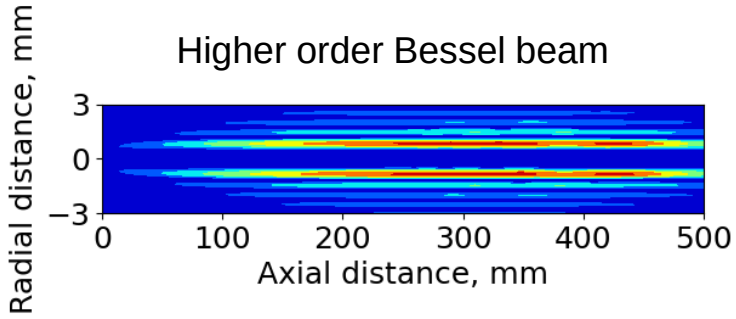

[1] Li, J. X., et al., Review of Scientific Instruments **89**(9), (2018)
[2] M. Massari, et al., Applied Optics, **54**(13), (2015)

Bessel overlap

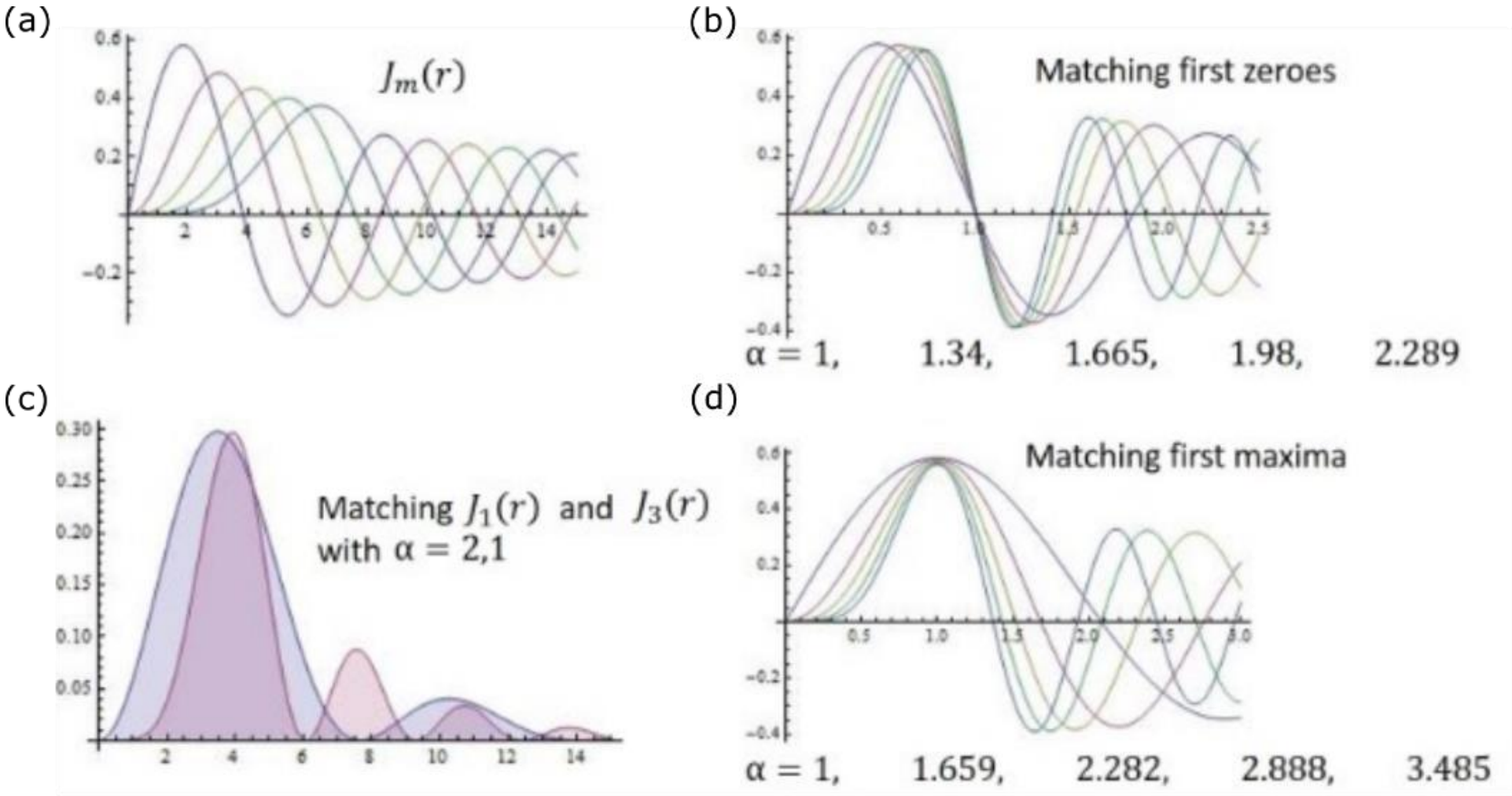

High aspect ratio chiral beams 1

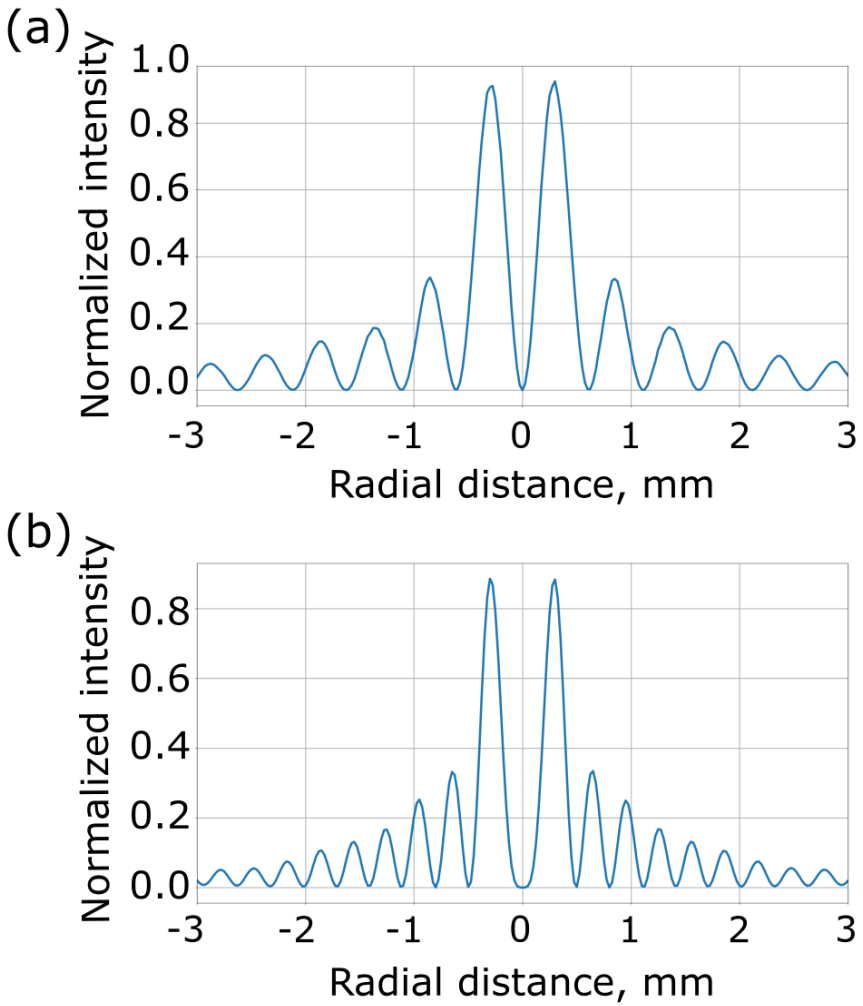

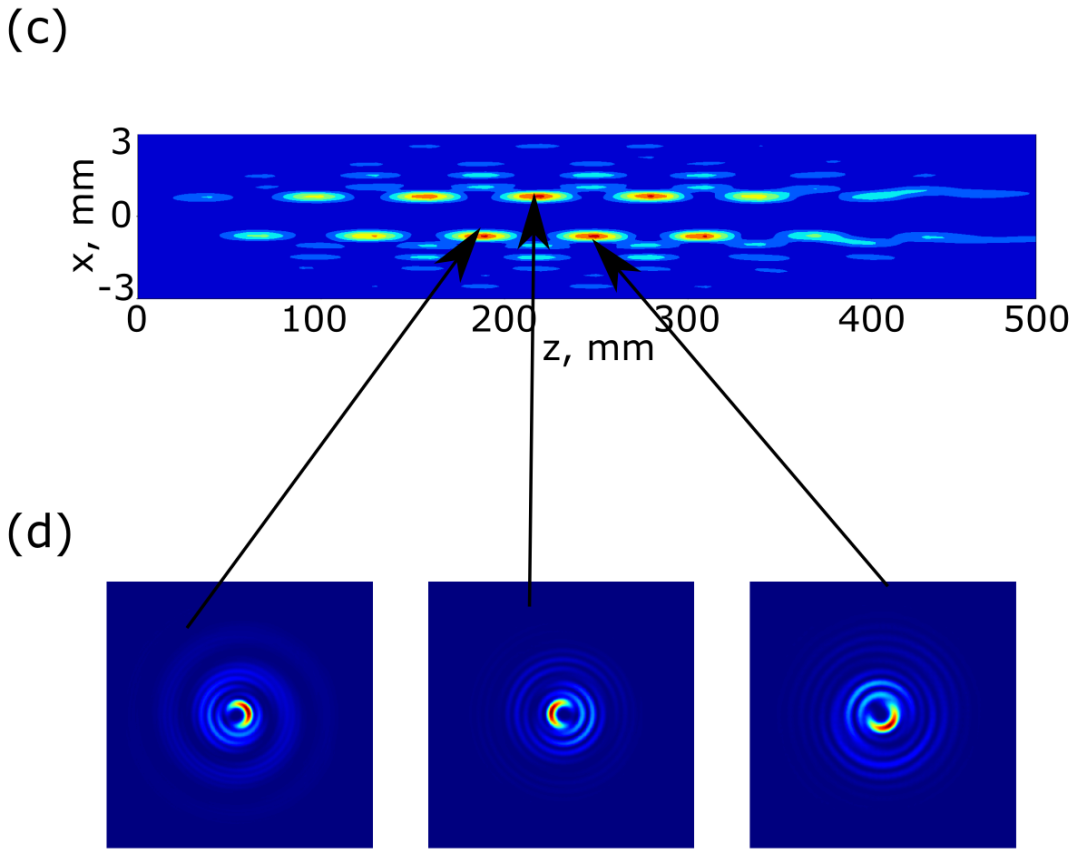

High aspect ratio chiral beams 2

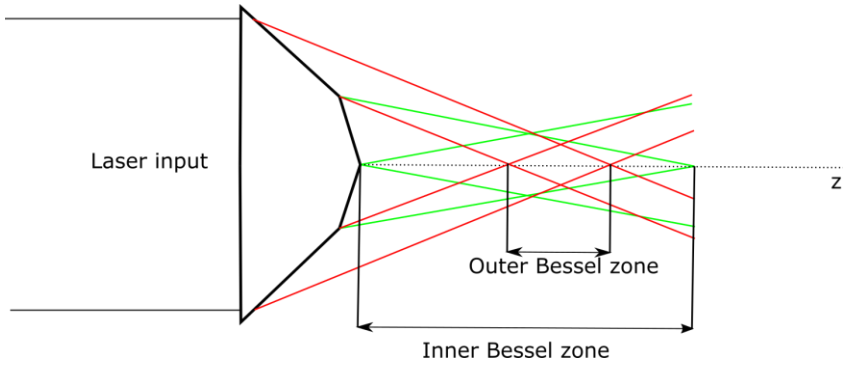

Fig. Schematic overlay of Bessel zones

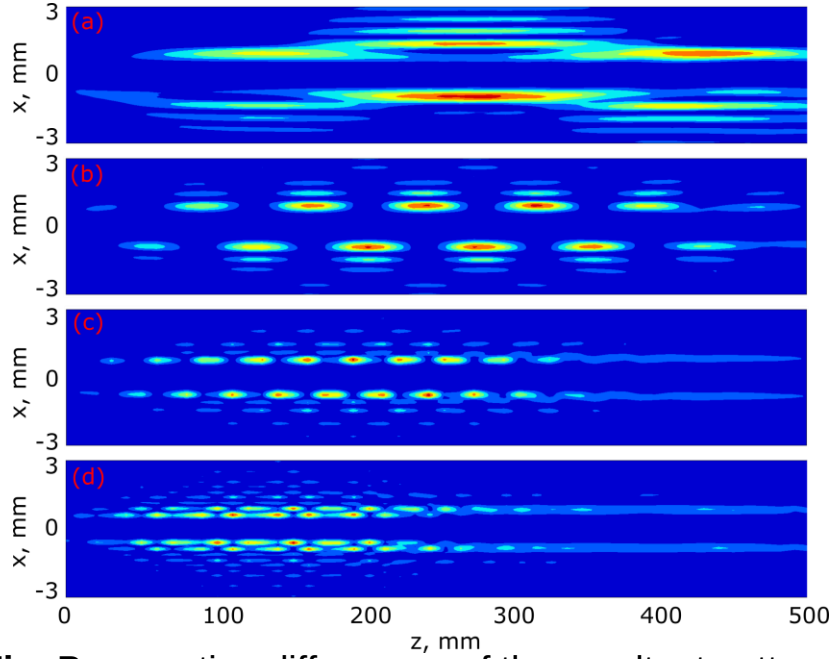

Fig. Propagation differences of the resultant pattern due to different axicon angle ratios: 1.1, 1.4, 1.8, 2.3.

$$\Delta l = l_2 - l_1$$

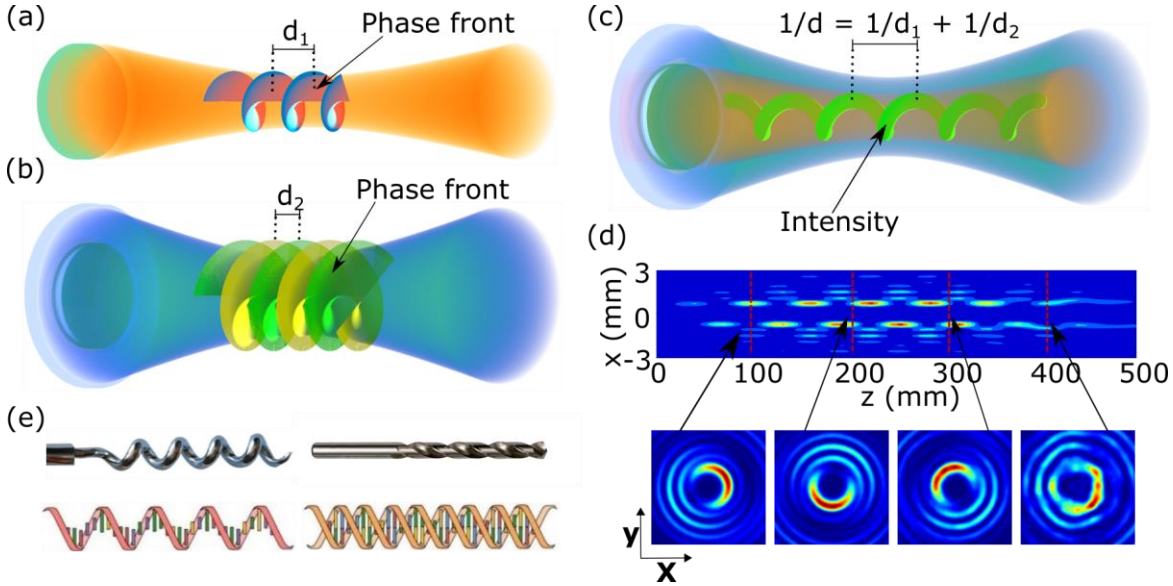

Fig. (a) Phase-helical Bessel beam with single helicity l_1 = 1, wavefront. (b) with double helicity l_2 = 2 wavefront. (c) Optical drill bit, emerging from the interference of beams a and b, showing a helical intensity distribution. (d) Axial XZ and transverse XY cross-sections of the simulated intensity distribution. (e) Examples with the same geometric structure to the proposed light intensity patterns.

Spatial light modulator - SLM

PLUTO-2.1 Spatial Light Modulator – Microdisplay Features	
Display Type:	Reflective LCOS (Phase Only)
Resolution:	1920 x 1080
Pixel Pitch:	8.0 µm
Fill Factor:	93 %
Active Area	15.36 x 8.64 mm (0.7” Diagonal)
Addressing	8 Bit (256 Grey Levels)
Signal Formats	HDMI – HDTV Resolution
Input Frame Rate	60 Hz

Spatial light modulator working principle

$$\Gamma = \frac{2\pi}{\lambda}\frac{OPL}{\cos\theta_{LC}}\left[\frac{1+(OPD/OPL)}{1+(OPD/OPL)\cos^2\phi}-1\right]$$

$$\phi(\theta_{inc},V) = \frac{\pi}{2}+\alpha(V)\mp\theta_{LC}(\theta_{inc})$$

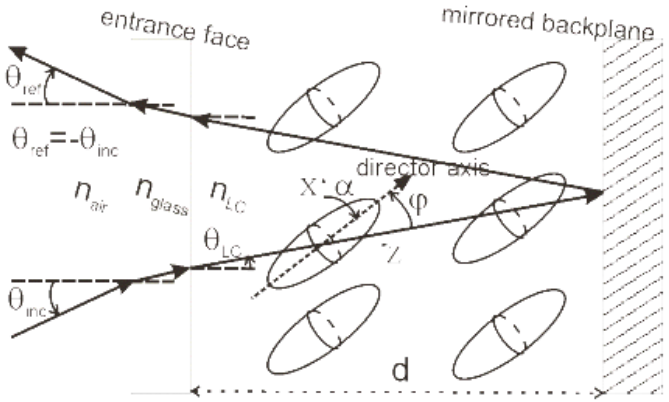

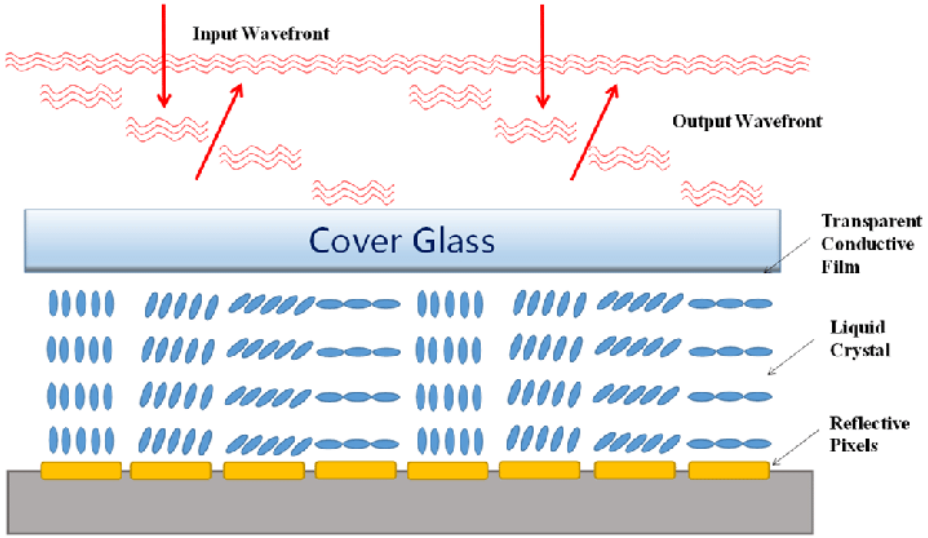

$$\phi = e^{i\frac{2\pi}{period}}$$

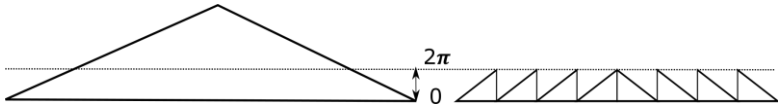

Fig. Comparison between a refractive and diffractive axicon

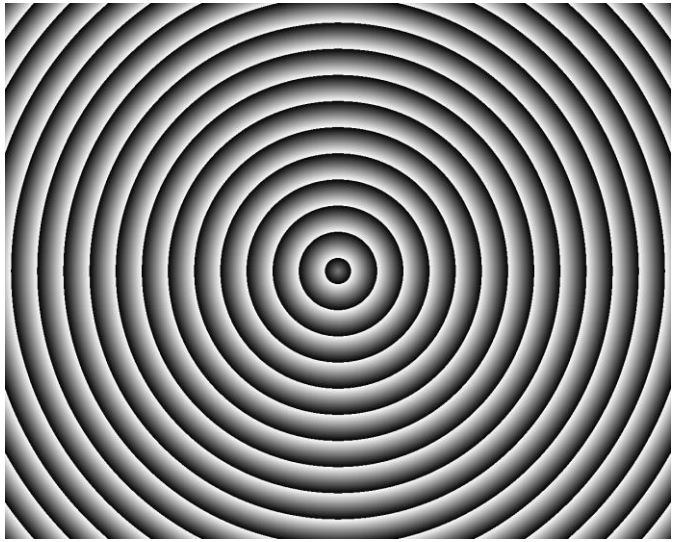

Fig. Axicon hologram

[1] Francés, Jorge, et al. *Optics express* 26.10 (2018): 12723-12741.

SLM beam modification methods

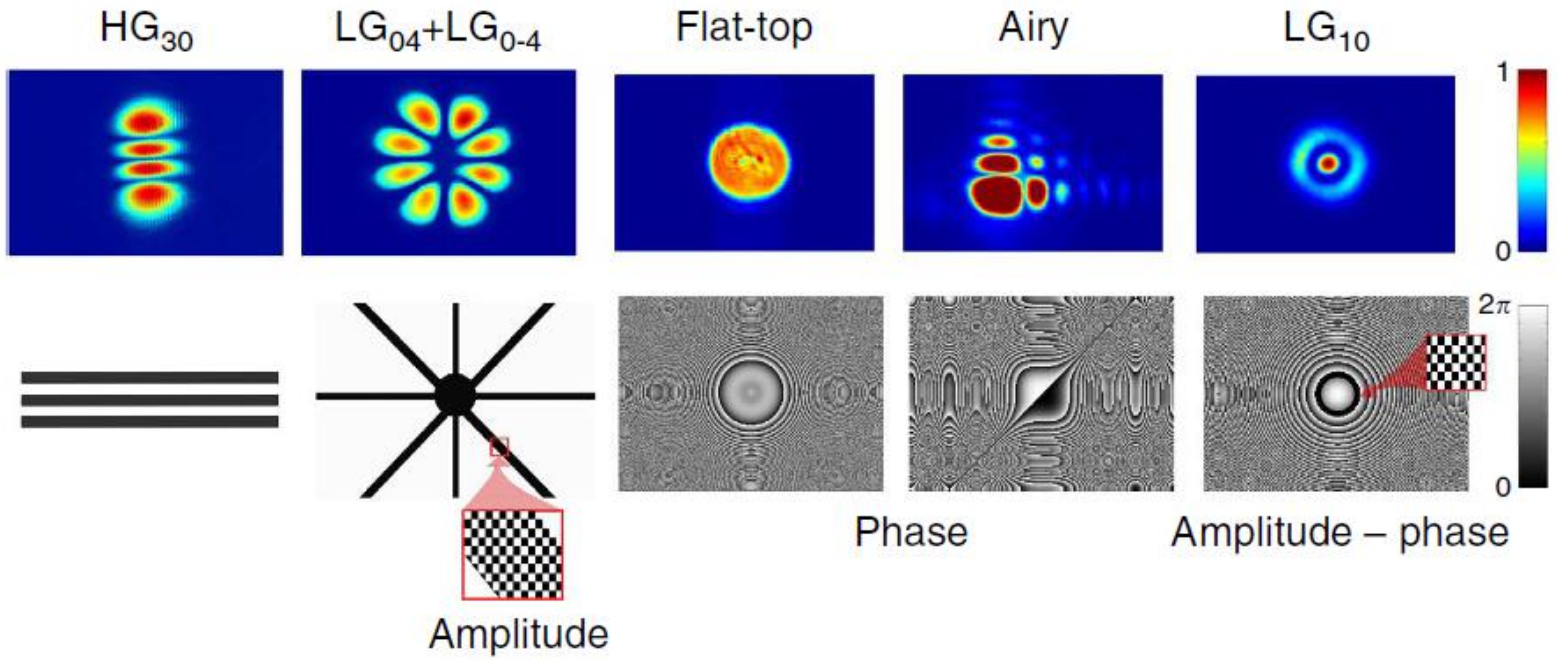

Fig. Examples of beam shaping variations to generate various intensity patterns.

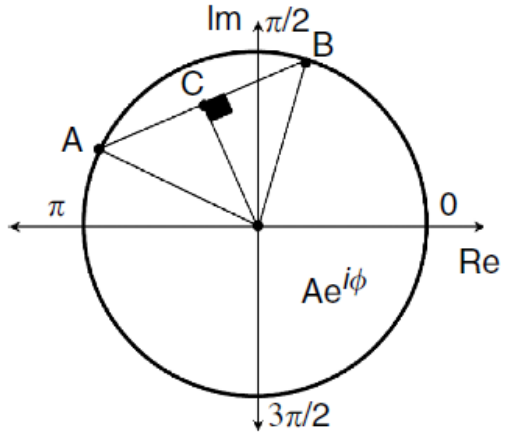

Fig. Complex plane of two nearby electric fields.

[1] Ngcobo, S., Litvin, I., Burger, L. *et al.*, *Nat Commun* **4,** 2289 (2013)

High aspect ratio chiral beams 3

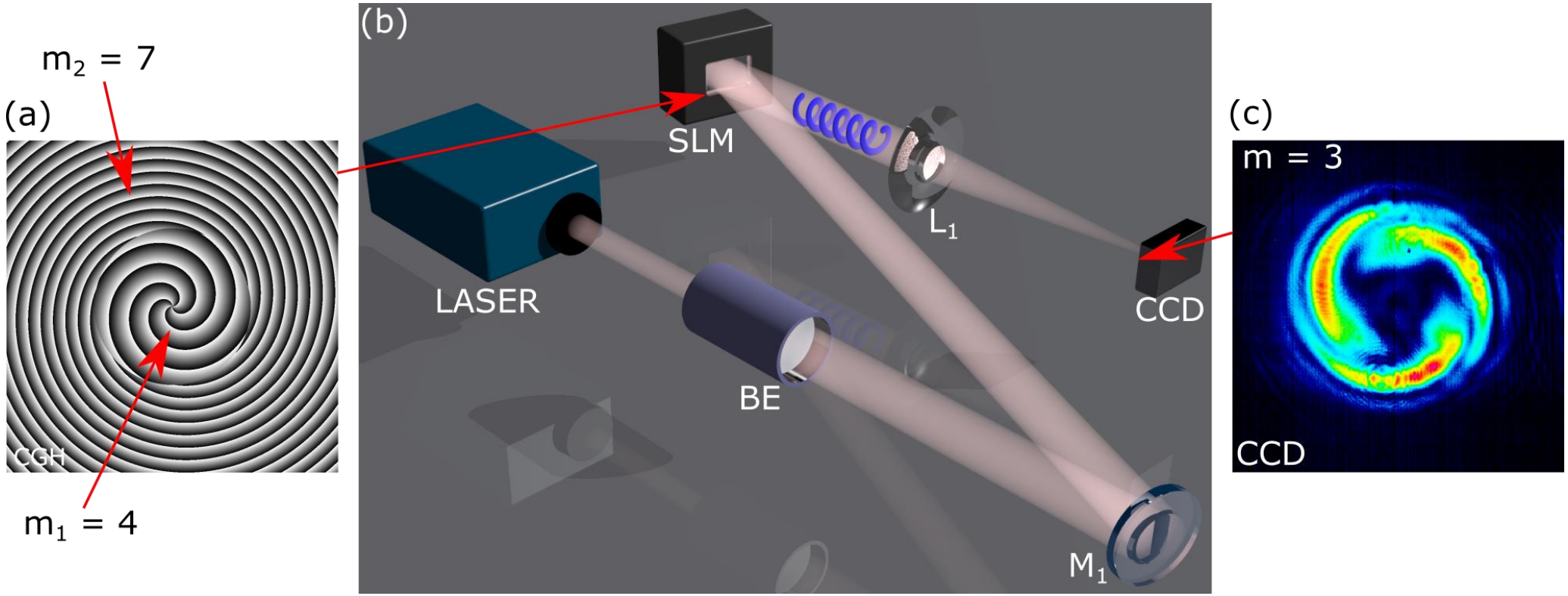

Fig. Optical scheme used for beam shaping. (a) Grayscale phase image of a computer-generated hologram displayed on the SLM (b) Optical chain (c) CCD captured intensity distribution

G. Kontenis et. al., Phys. Rev. Applied 17, 034059 (2022).

High aspect ratio chiral beams 4

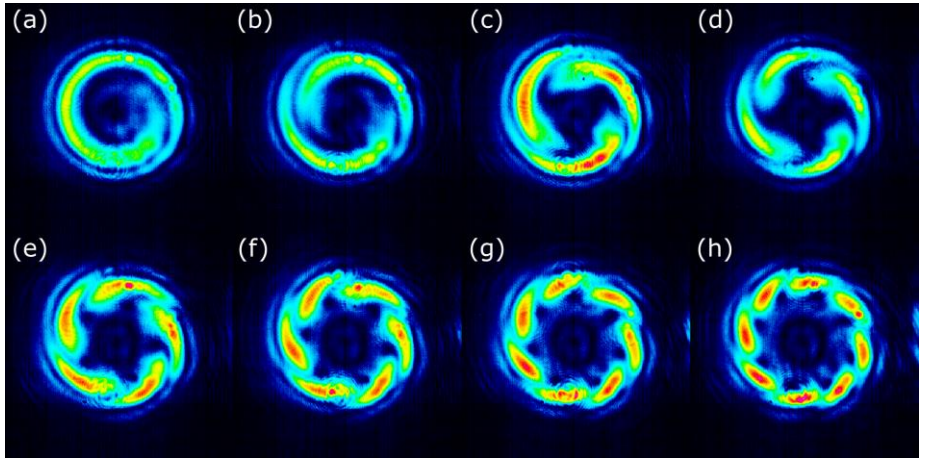

Fig. Intensity distribution with $l_1 - \text{constant}$

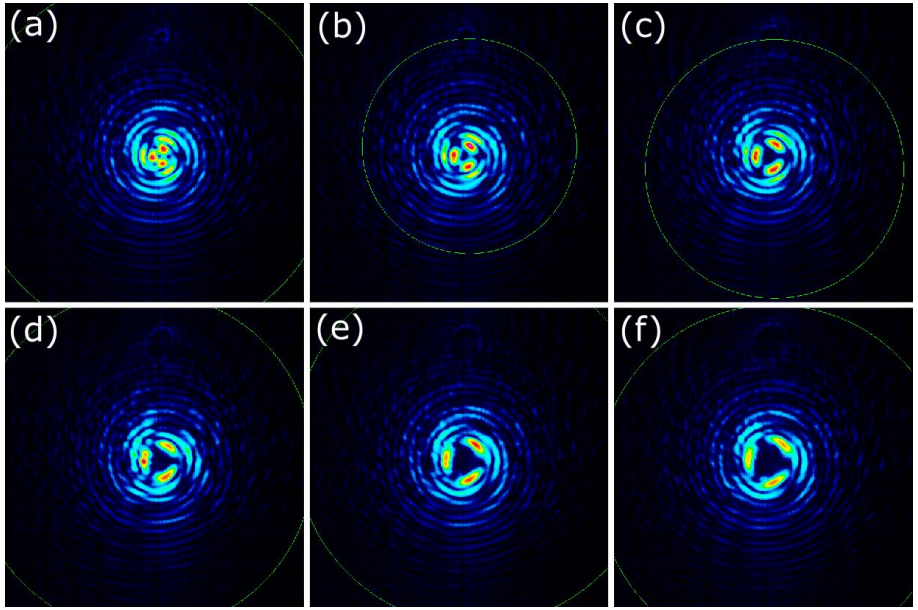

Fig. Intensity distribution with $\Delta l - \text{constant}$

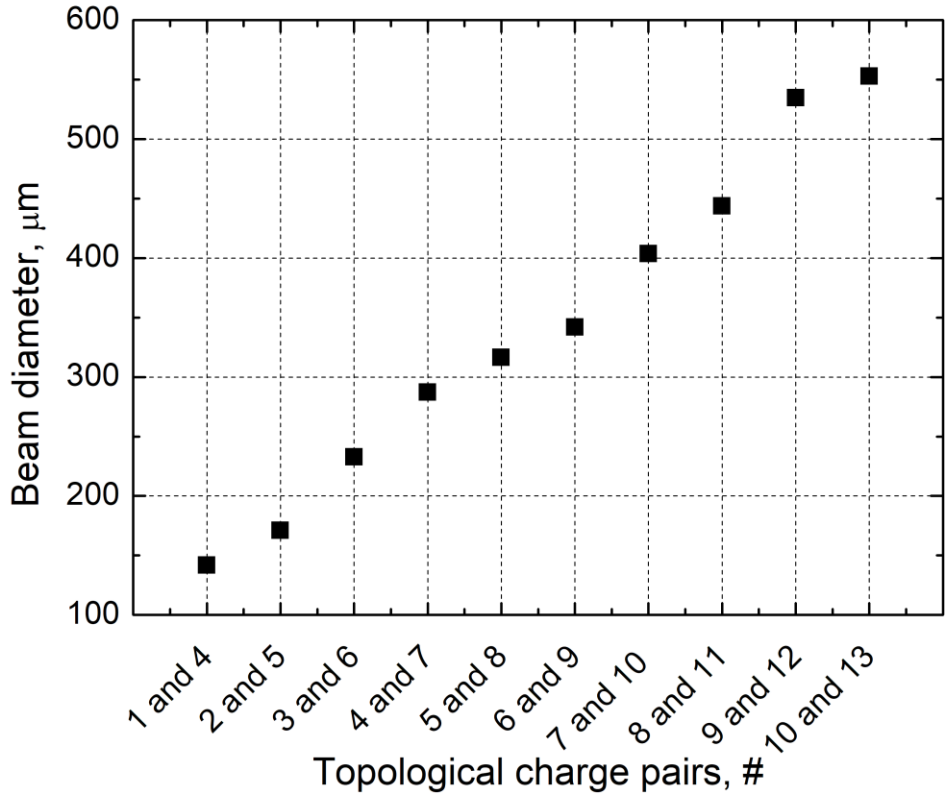

Fig. Structured beam diameter change with an increase in base topological charges

3D reconstruction

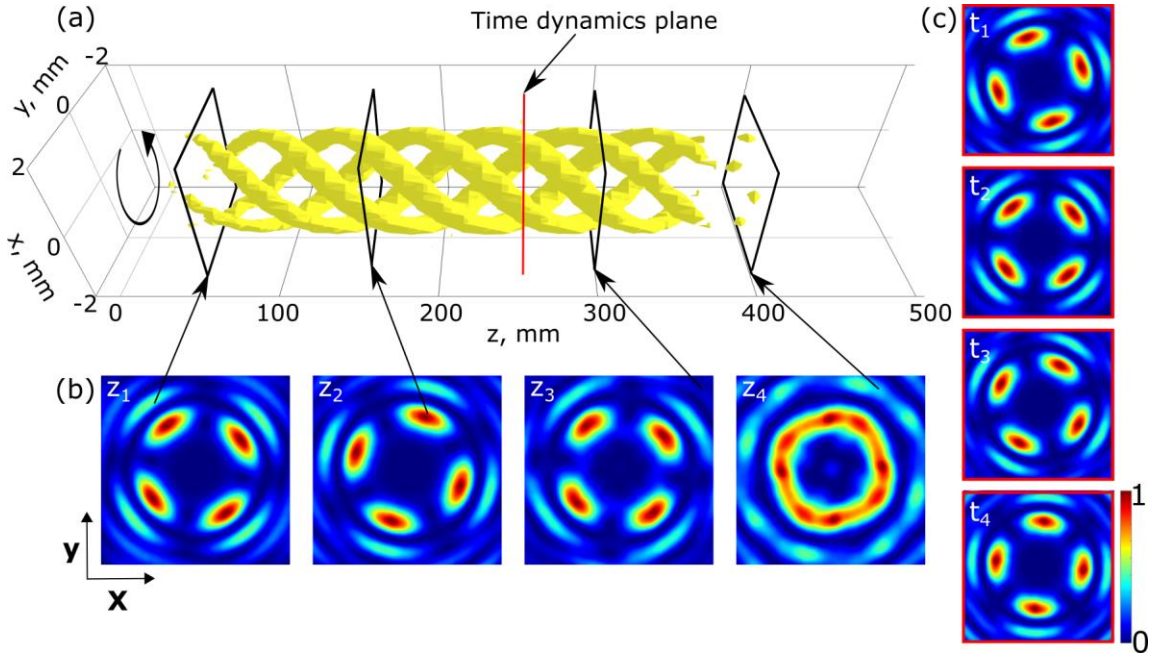

Fig. Numerical 3D isosurface of the interefering higher-order Bessel beams

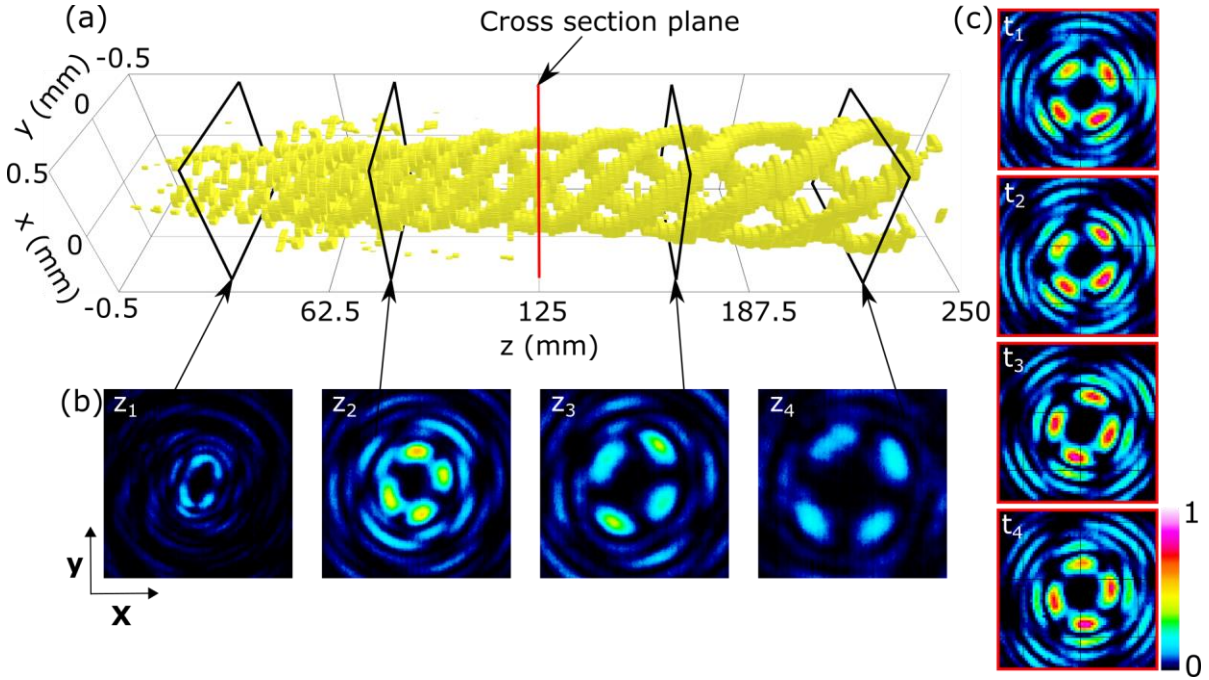

Fig. Experimental 3D isosurface of the interefering higher-order Bessel beams

Time dynamics

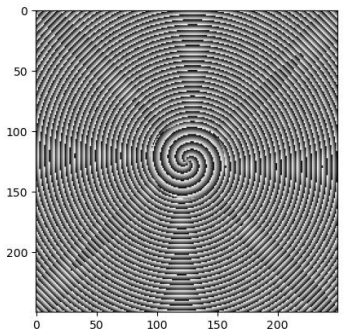

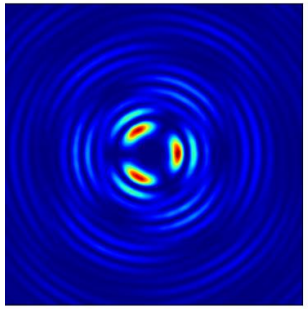

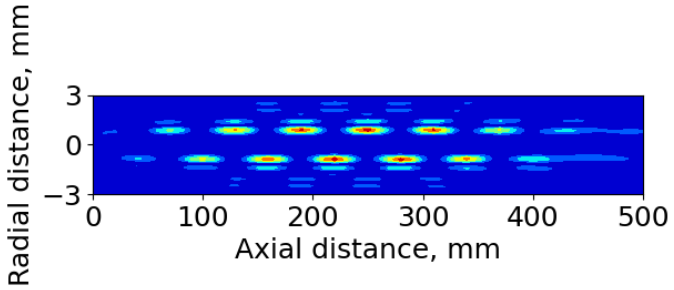

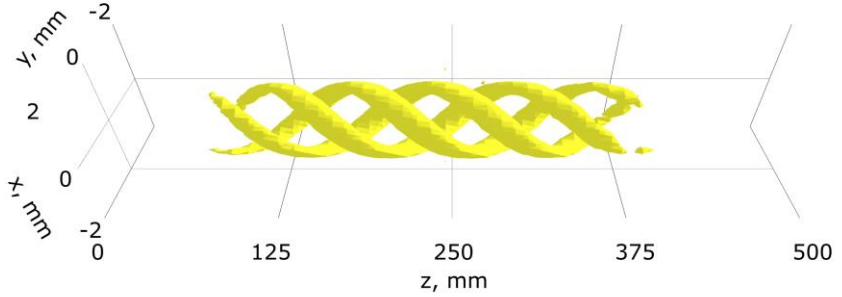

Liuminescence of the beam

- Rhodamine B dye as fluorescent material,
- 4F system with 150 mm lens and 0.2 NA objective for focusing the beam,
- Microscope of 0.65 NA and 100 mm lens for visualization.

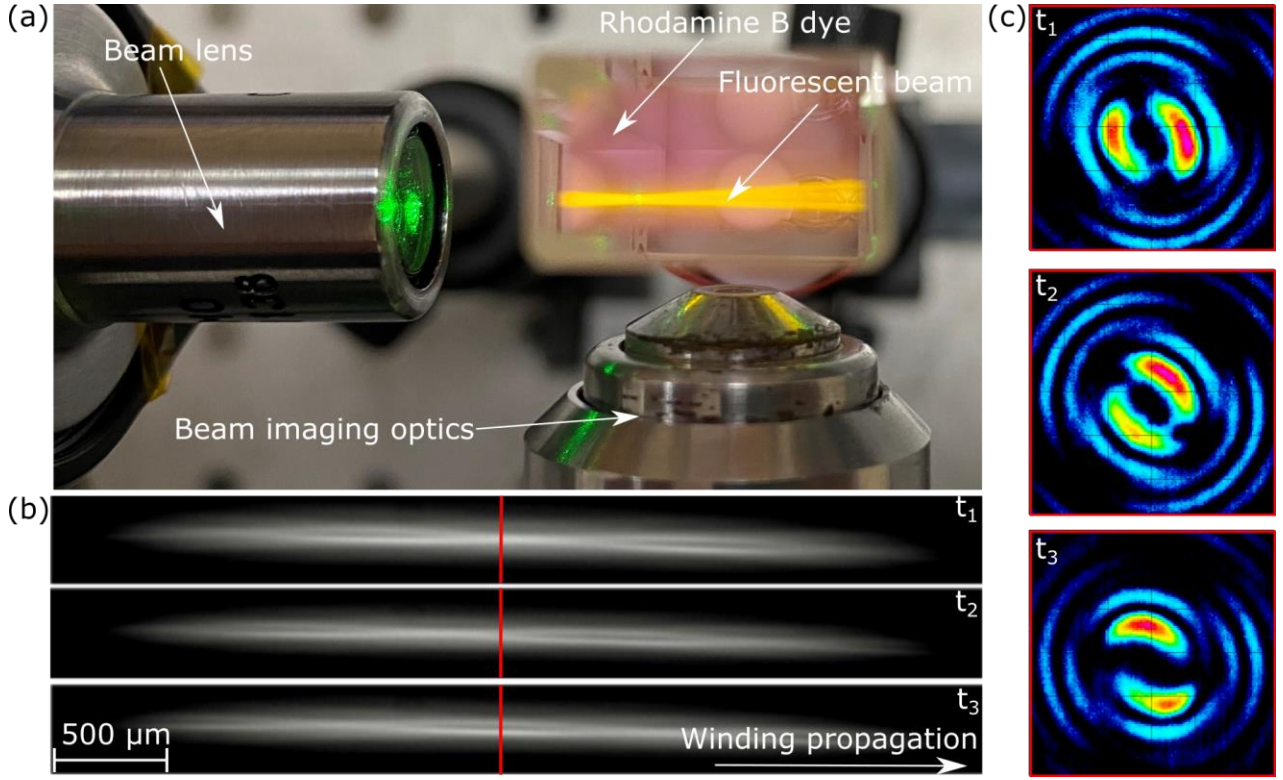

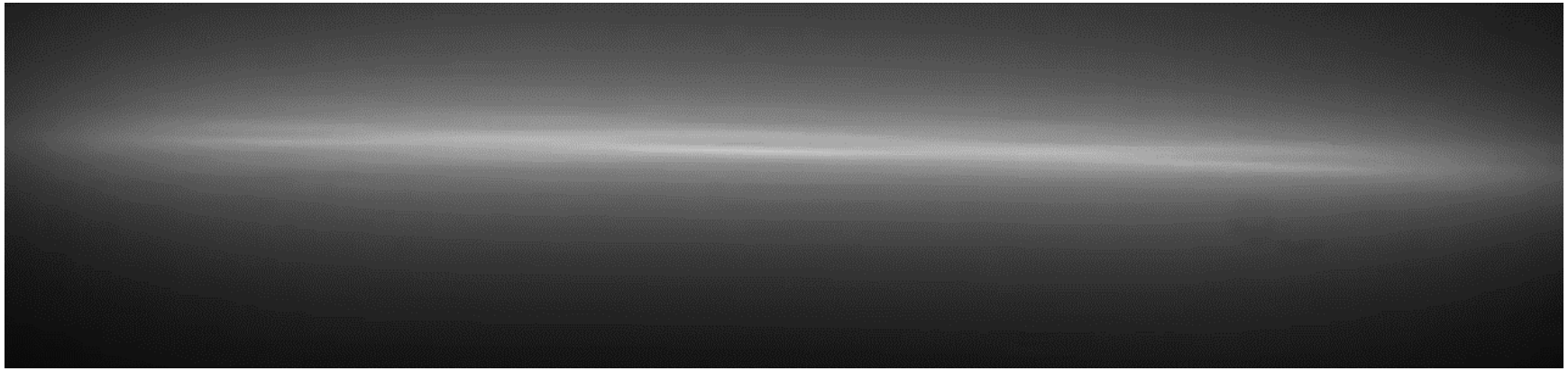

Pulse beating

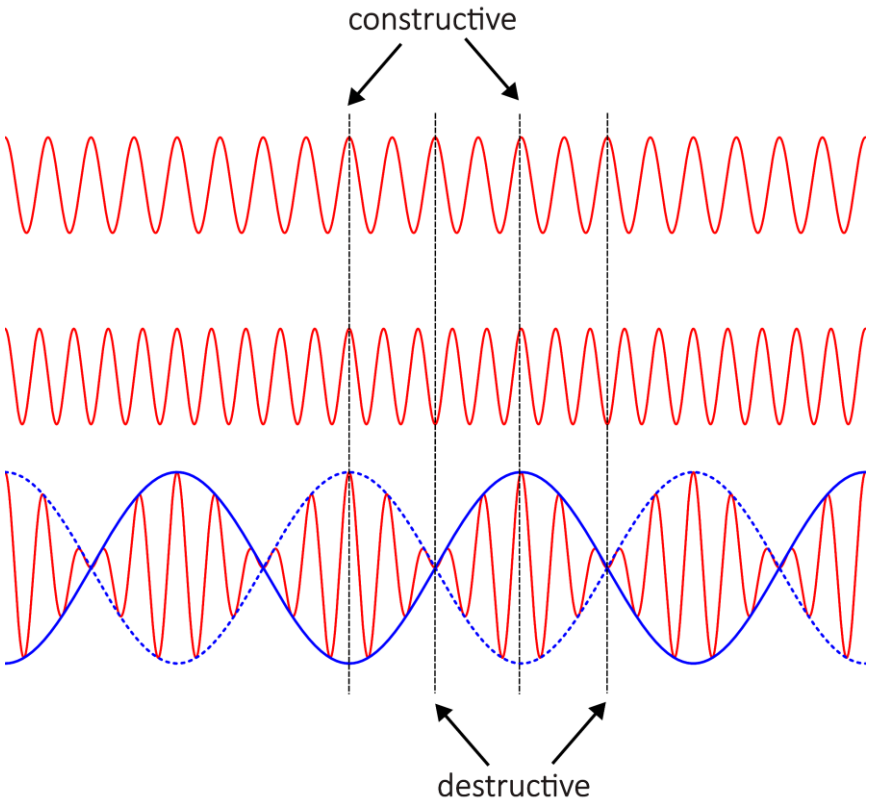

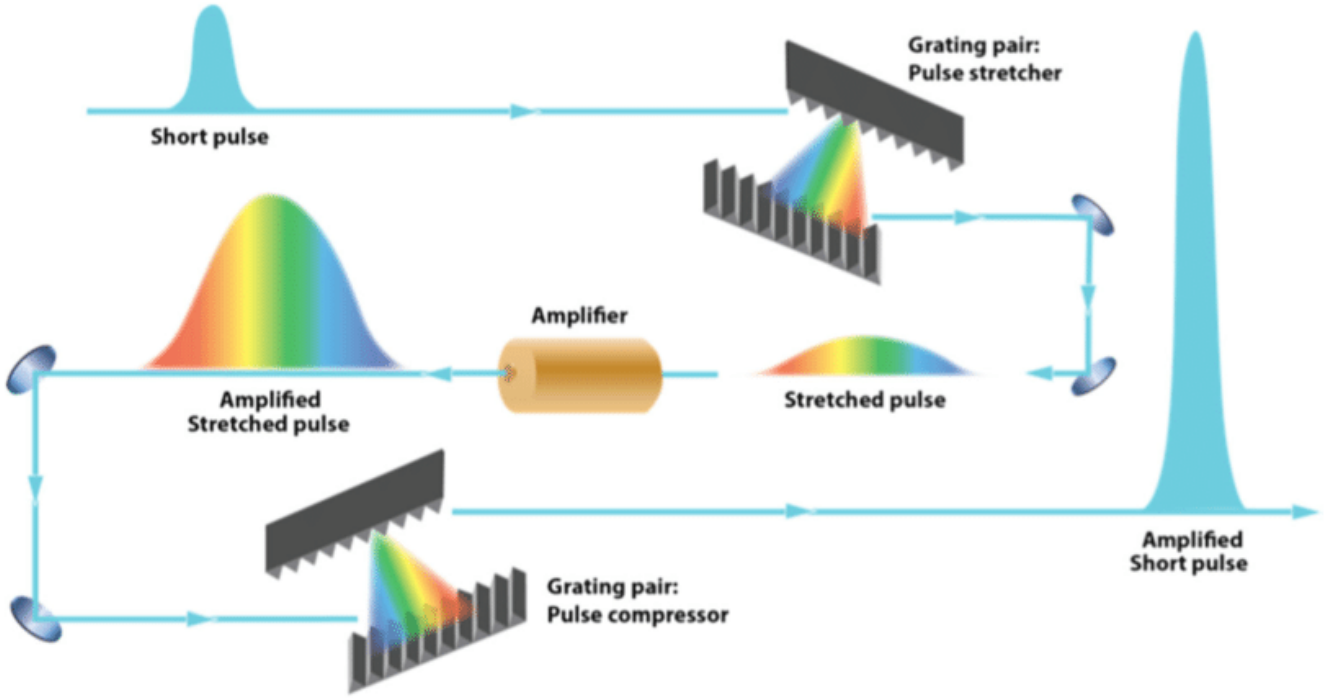

[1] https://phys.libretexts.org/Courses/University_of_California_Davis/UCD%3A_Physics_7C_-_General_Physics/8%3A_Waves/8.6%3A_Beats (image searched on 2025 March 25)
[2] M. C. Asplund, J. A. Johnson & J. E. Patterson, "The 2018 Nobel Prize in Physics: optical tweezers and chirped pulse amplification", Anal. Bioanal. Chem., vol. 411 (3), 5001-5005 (2019).

Helical beam formation from chirped pulses

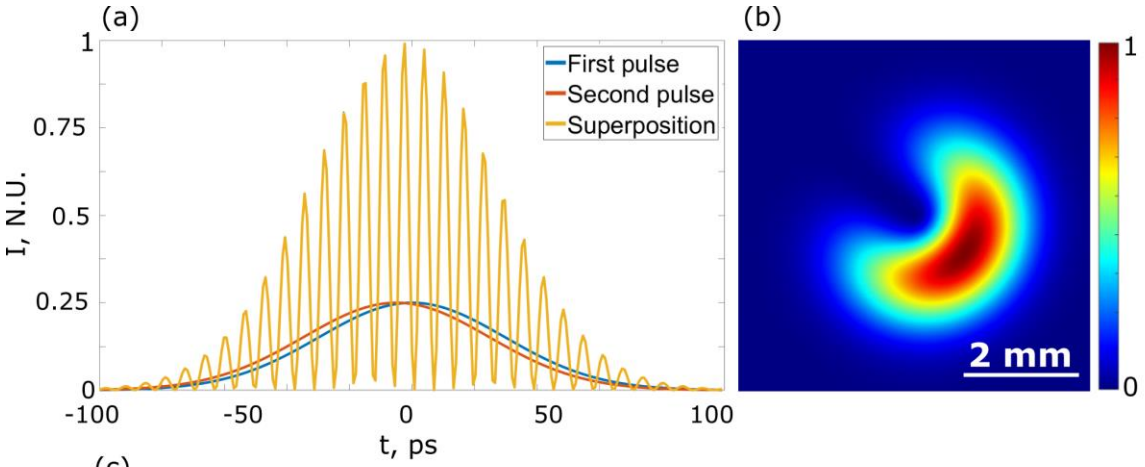

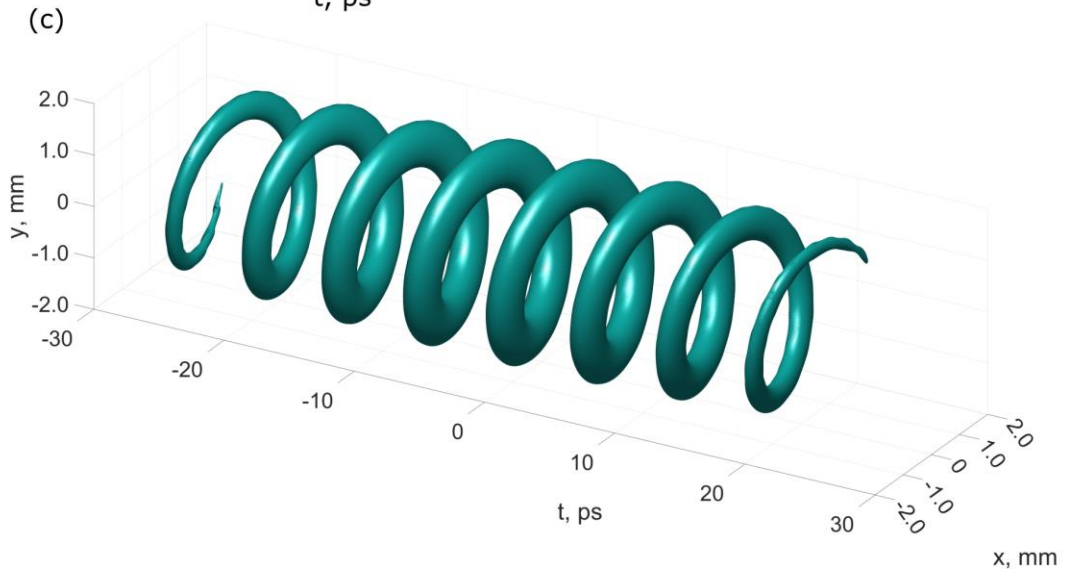

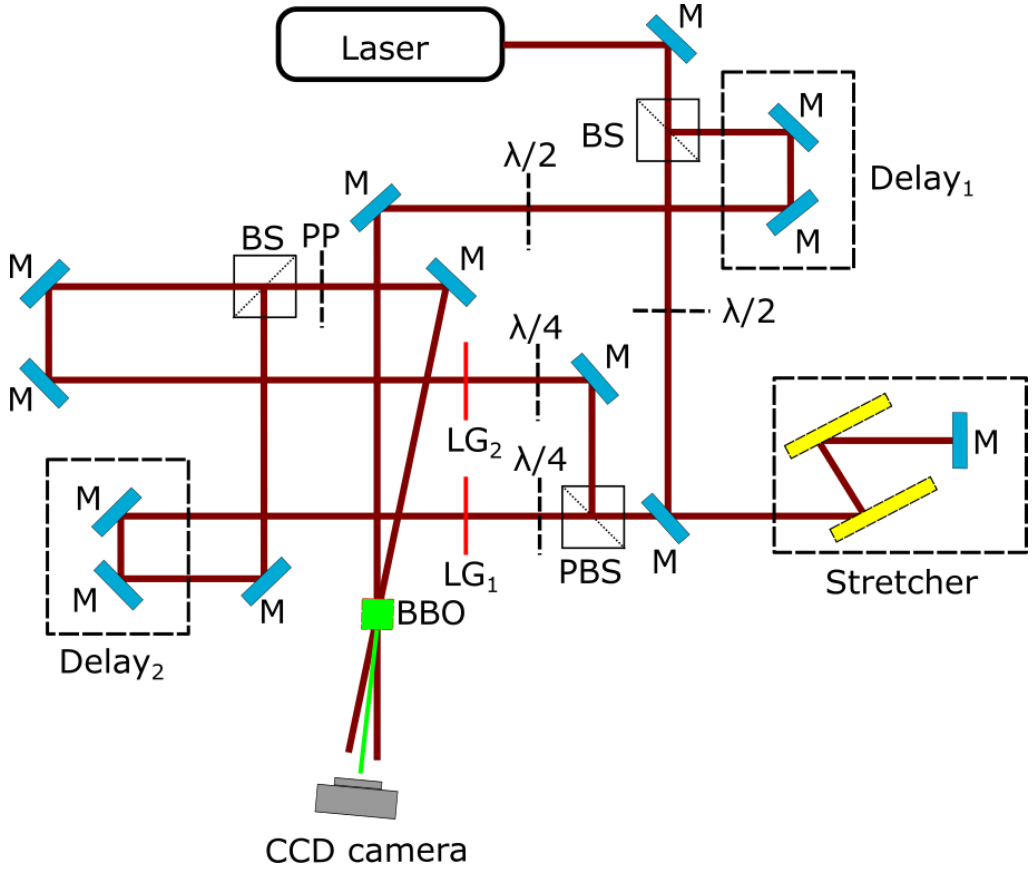

$$E_{\mathrm{p}} = \mathrm{e}^{-\frac{(t+T_{\mathrm{shift}})^2}{\tau_{chirp}^2}(1+i\gamma)}$$

$$\gamma = \sqrt{\left(\tau_{\mathrm{chirp}}/\tau_0\right)^2 - 1}$$

$$T_{period} = \frac{\pi\tau_{chirp}^2}{T_{shift}\sqrt{\frac{\tau_{chirp}^2}{\tau_0^2} - 1}}$$

G. Kontenis, et. al., Lithuanian Journal of Physics 63(3), 113–120 (2023).

Differences between harmonics

Vid. Delay line translation at a speed of 10 μm/s.

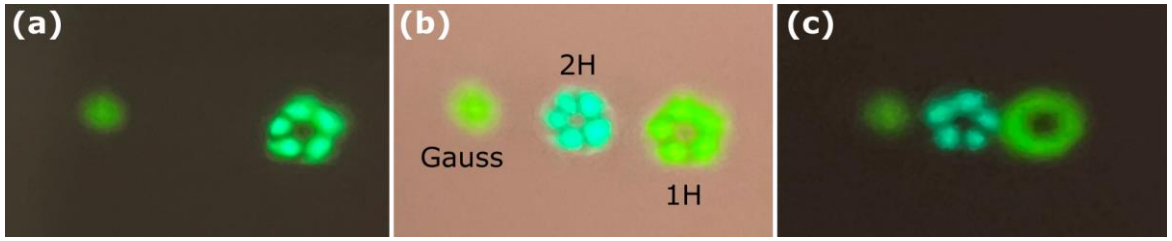

Fig. Luminescence of the beams on a "Thorlabs" beam visualizer.

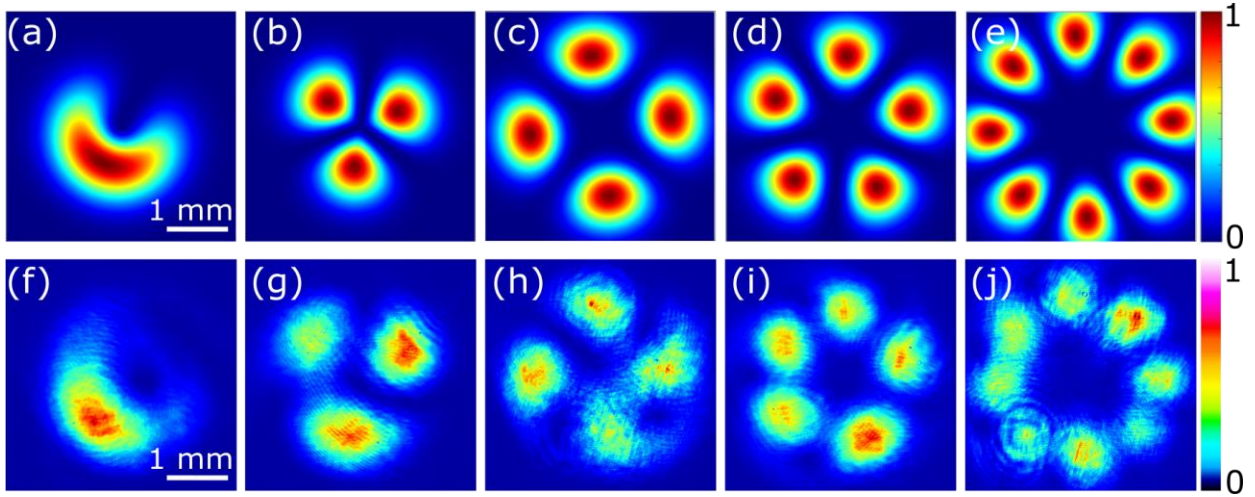

Fig. XY cross-section comparison of numerically simulated and experimentally measured intensity patterns of 2H generation between a Gaussian pulse and two interfering chirped beams.

Characterization of the beam

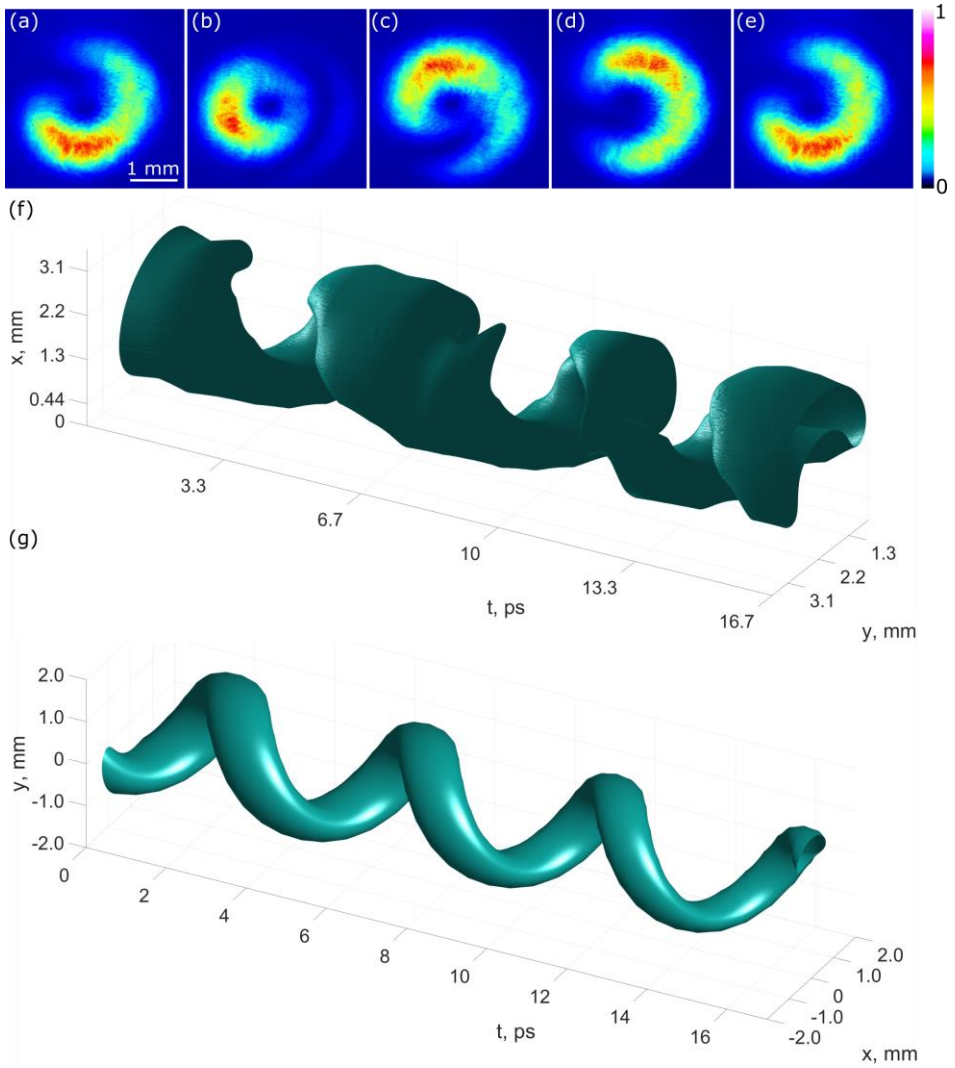

Fig. 3D reconstruction of (f) experimental and (g) numerical intensity distribution. Parameters: $T_{delay} = 6.67\ ps$, $\tau_0 = 200\ fs$, $\tau_{pulse} = 70\ ps$

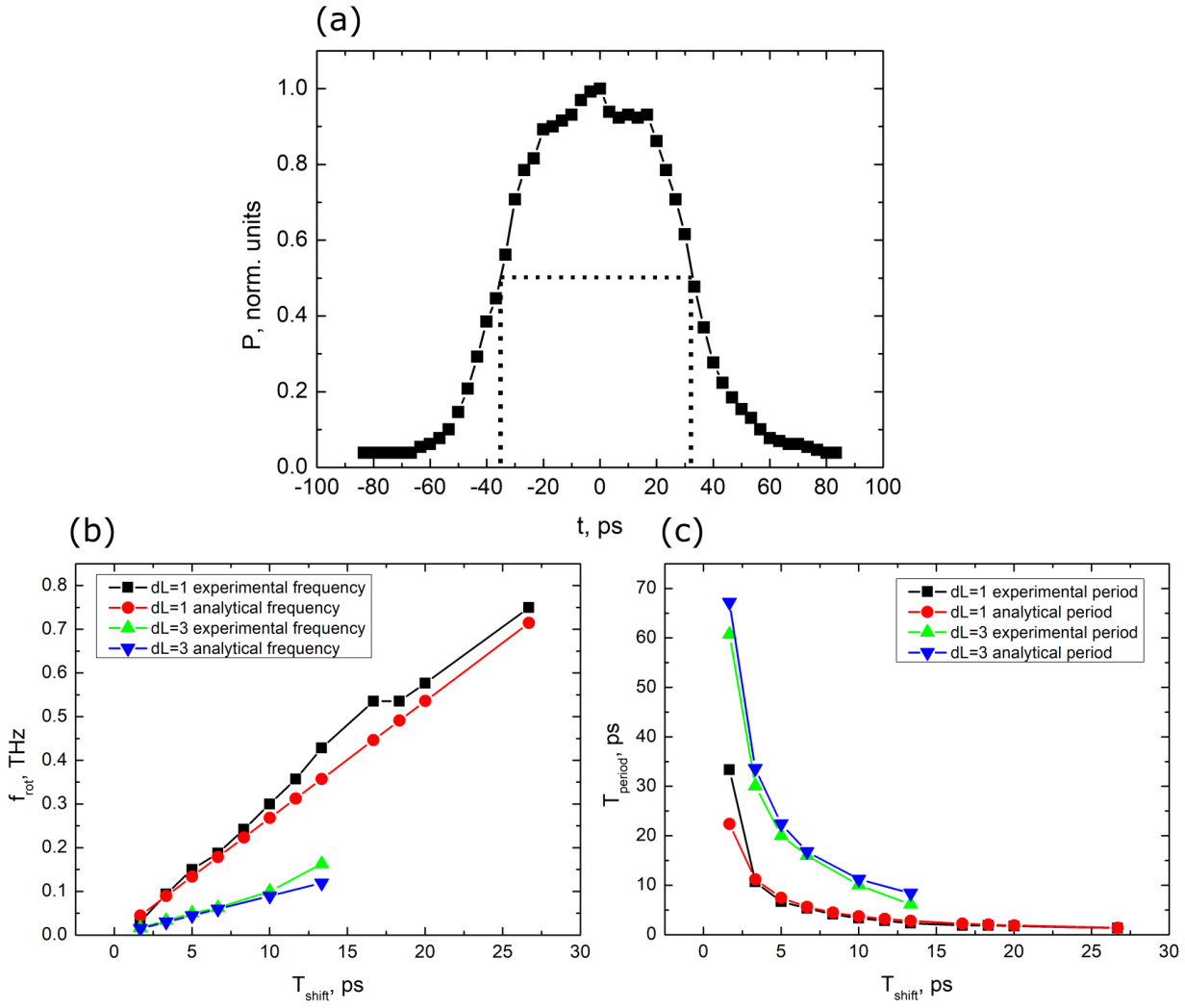

Fig. (a) chirped pulse duration (b) (c) are rotation frequency and period dependence on delay between pulses. $\tau_{pulse} = 70\ ps$

Alignment

Energy

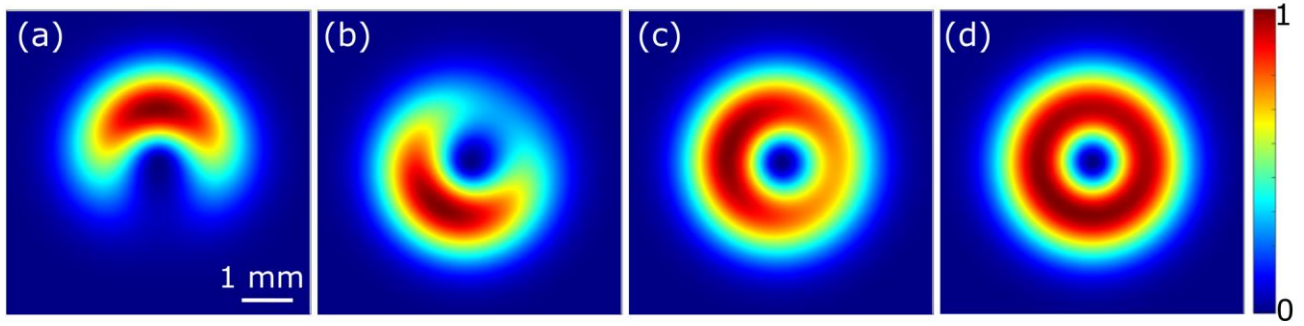

Fig. Simulated XY intensity distributions of a Δ*l* = 1 helical structure with a pulse delay between interfering beams of 25, 50, 75, 100 ps respectively.

Angle

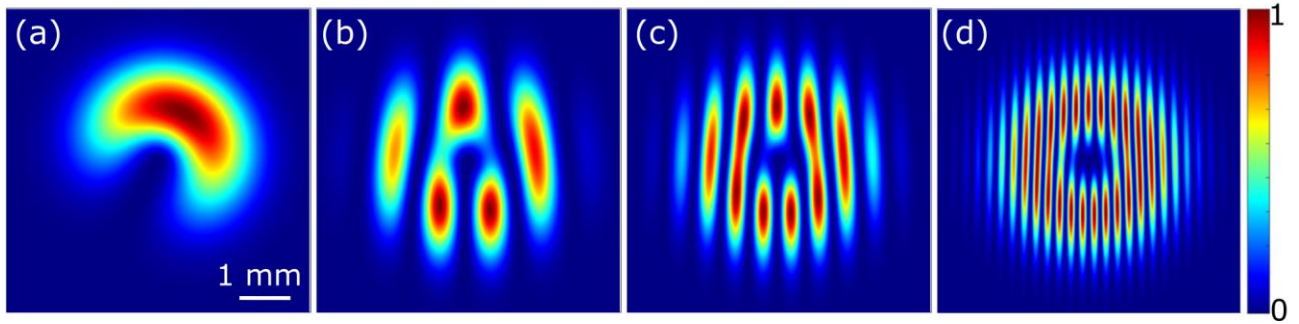

Fig. Simulated XY intensity distributions of a Δ*l* = 1 helical structure with propagation angles between interfering beams of 0, 0.05, 0.1, 0.25 deg respectively. The pulse shift was 2 ps.

Limitations of helical intensity beam formation

- Both beams are propagating in the same direction at the same speed
- The structure is formed within it
- Due to the same phase relationship between the pulses the twisted structure is static

Overlap increases

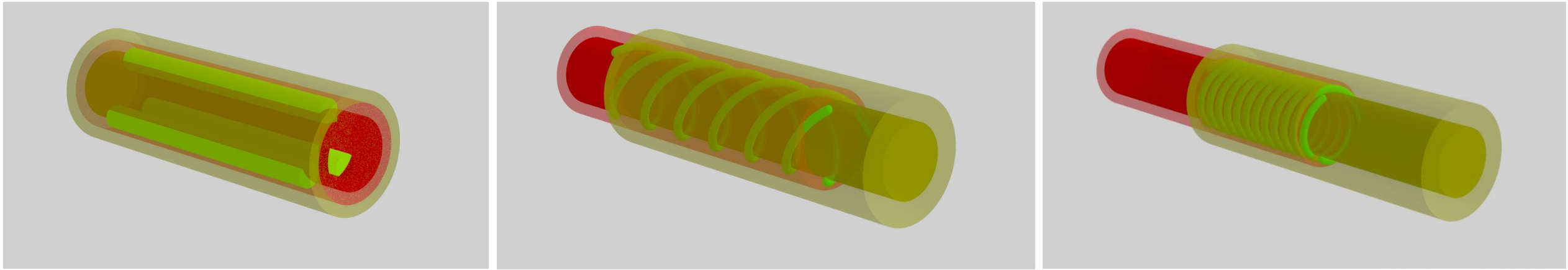

Rotation speed increases

Fabrication methods

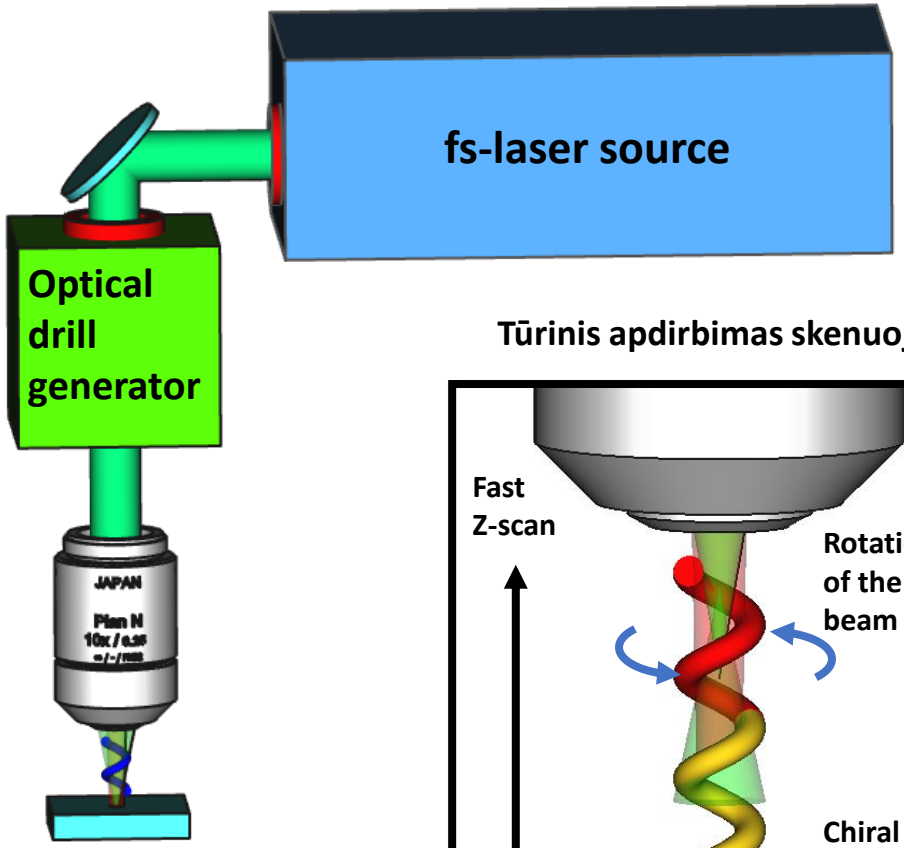

Tūrinis apdirbimas skenuojant

Surface machining

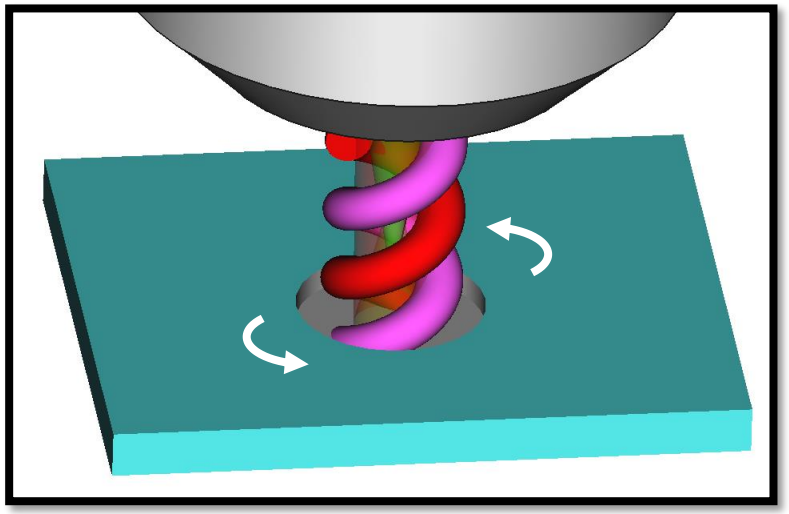

Fast rotating temperature gradient

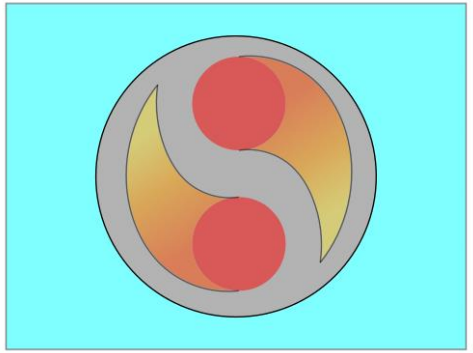

Relation of THz rate burst pulses and the *optical drill*

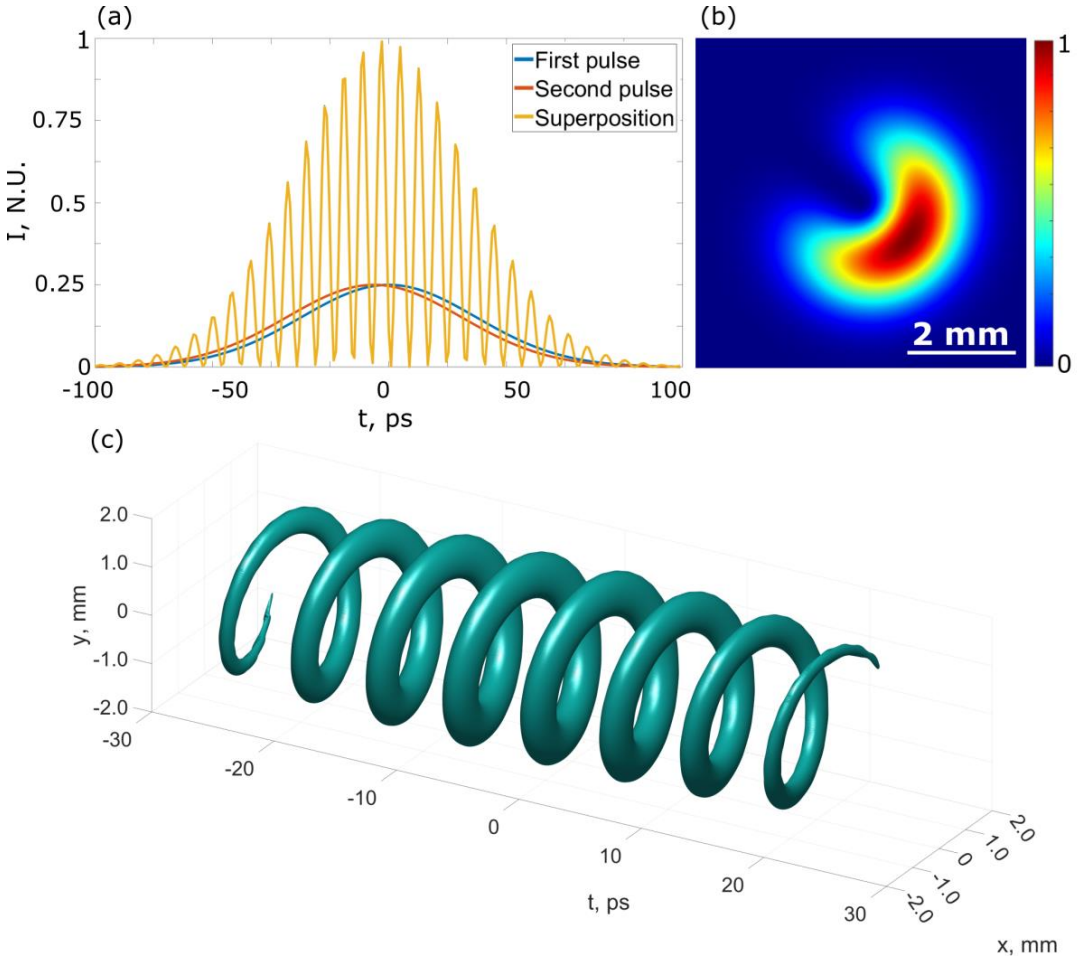

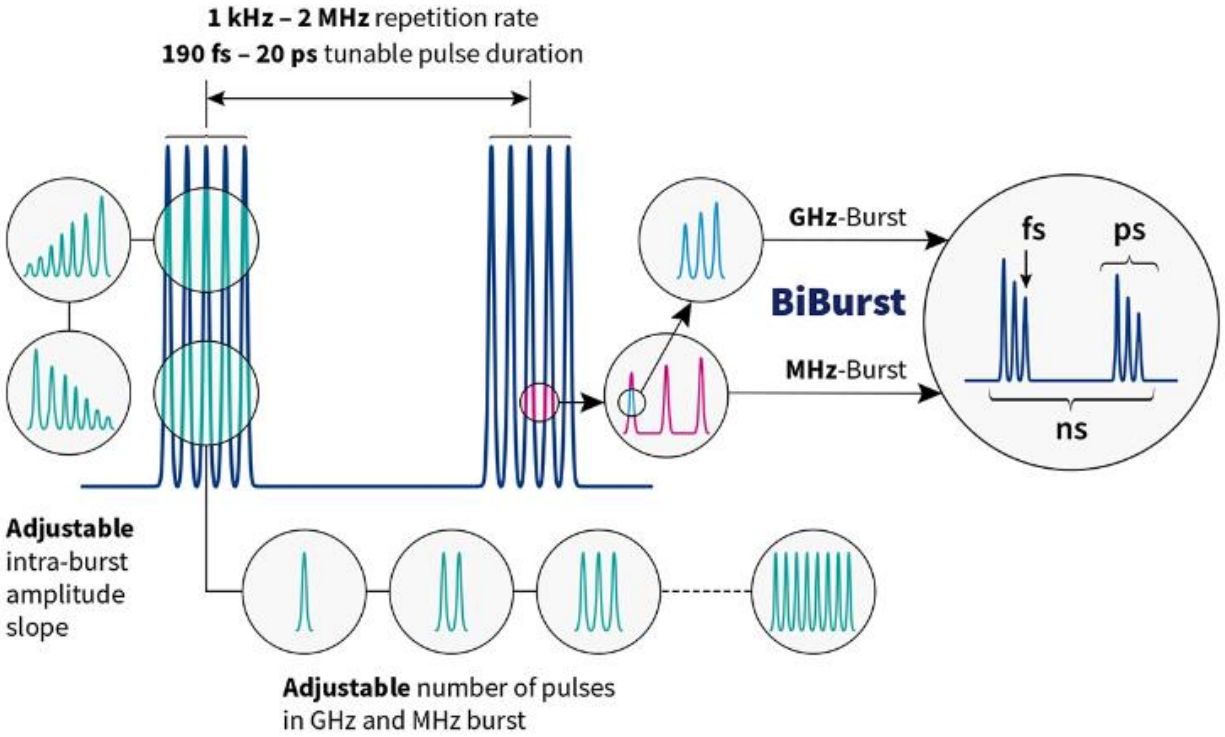

Figure 1: Operating diagram of tunable GHz and MHz burst with Burst-in-Burst capability

[1] Light conversion, "GHZ/MHZ FEMTOSECOND BURST FOR ENHANCED MATERIAL PROCESSING", (Image searched 2024 July 3)

Resultant ablated regions

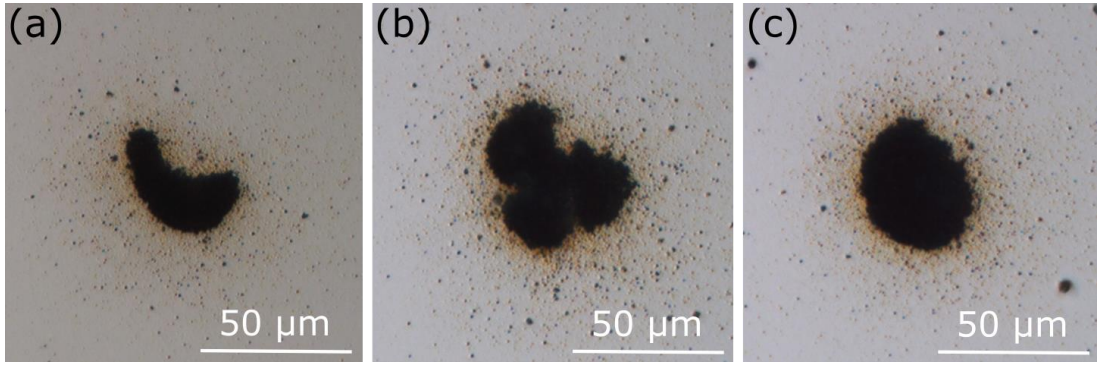

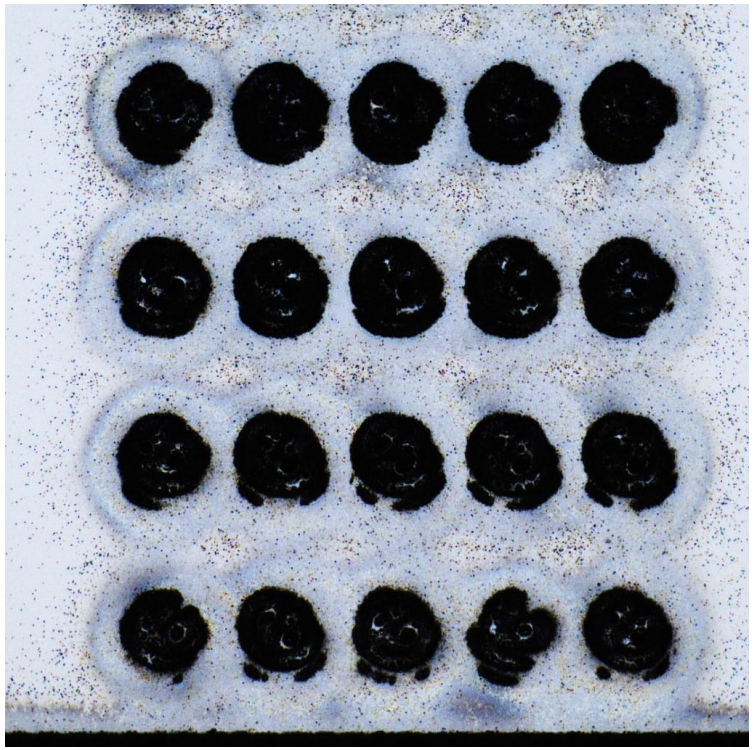

Fig. Ablation zone brightfield image

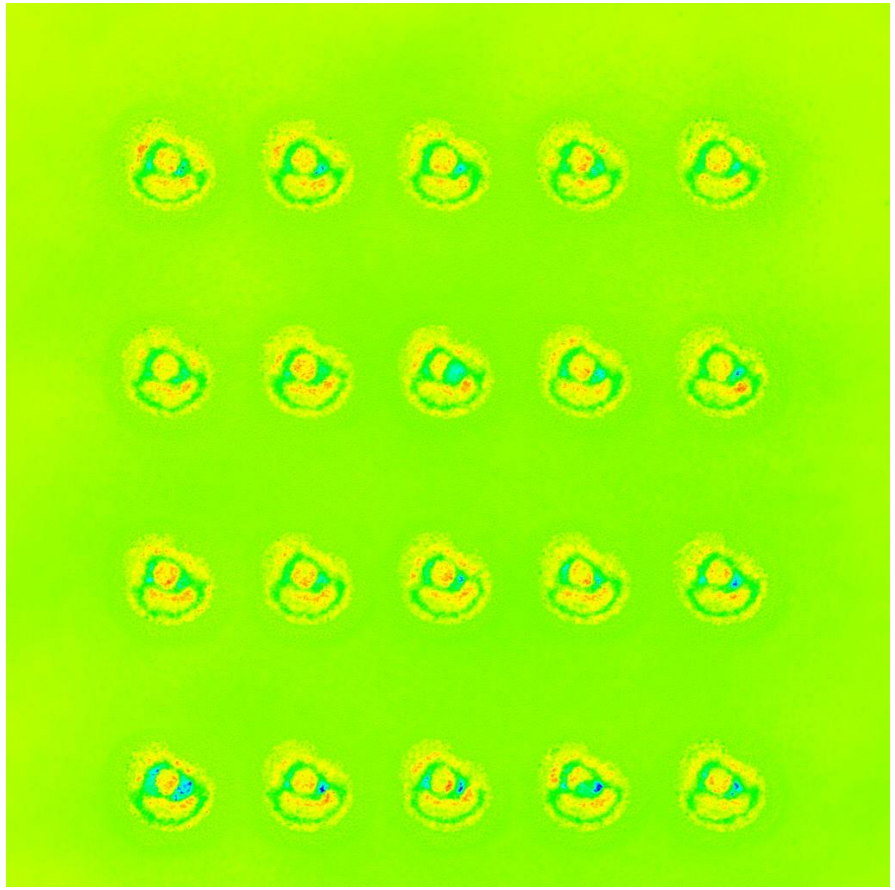

Fig. Ablation zone height map

Ablation zone evaluation

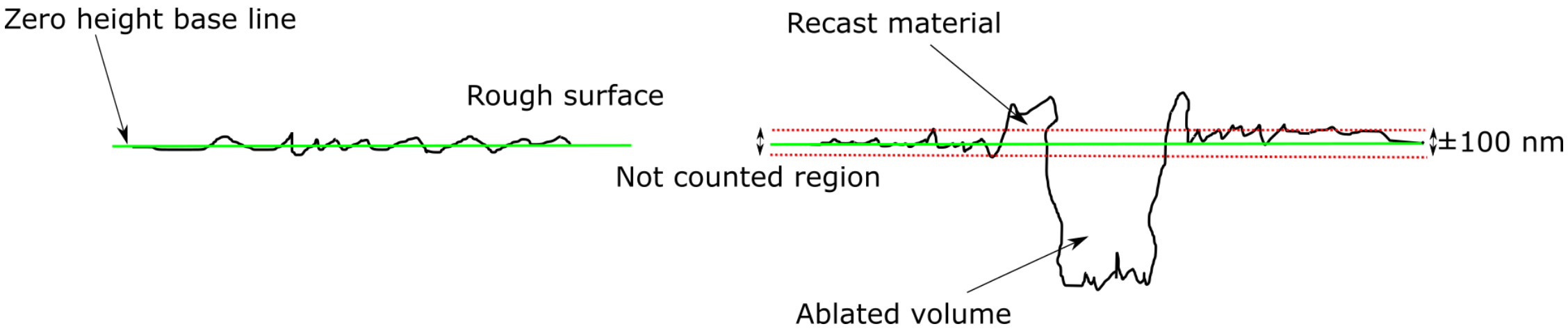

Fig. Ablated volume calculation scheme. Rough region around the base line is ignored for the calculation.

Light-matter interaction 1

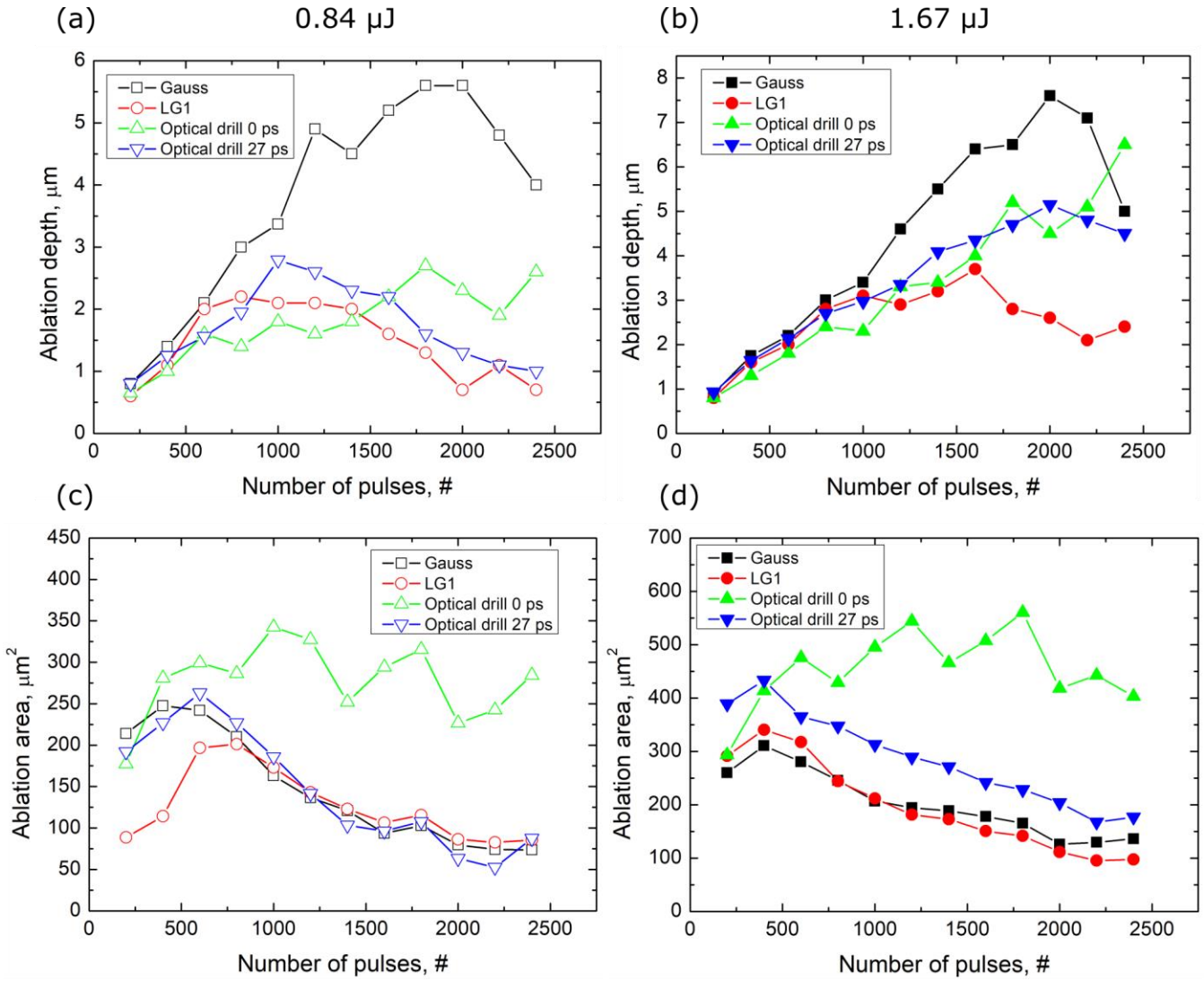

Fig. Ablation depth and ablation area of silicon wafer from the number of pulses with different spatial beam shapes.

G. Kontenis et. al., Optics & Laser Technology, (2025)

Light-matter interaction 2

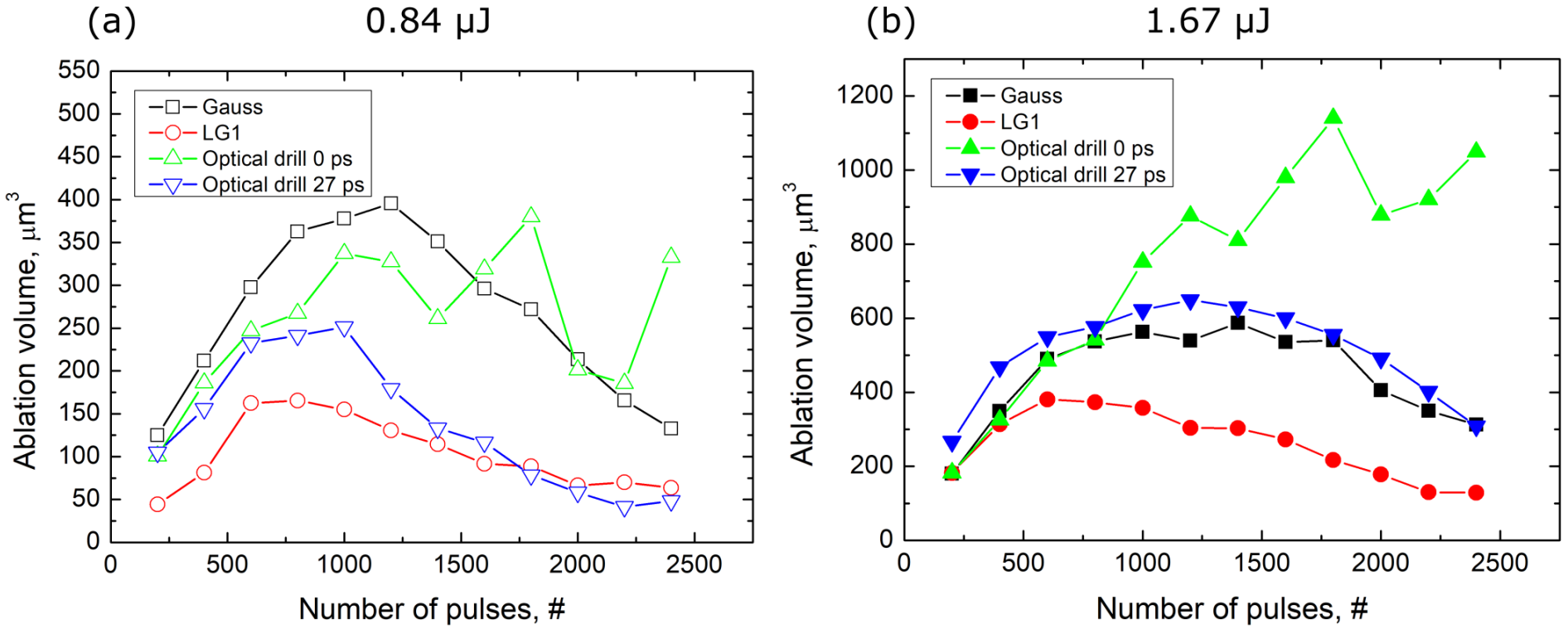

Fig. Ablated volume from the number of pulses with different spatial beam shapes.

Light-matter interaction 3

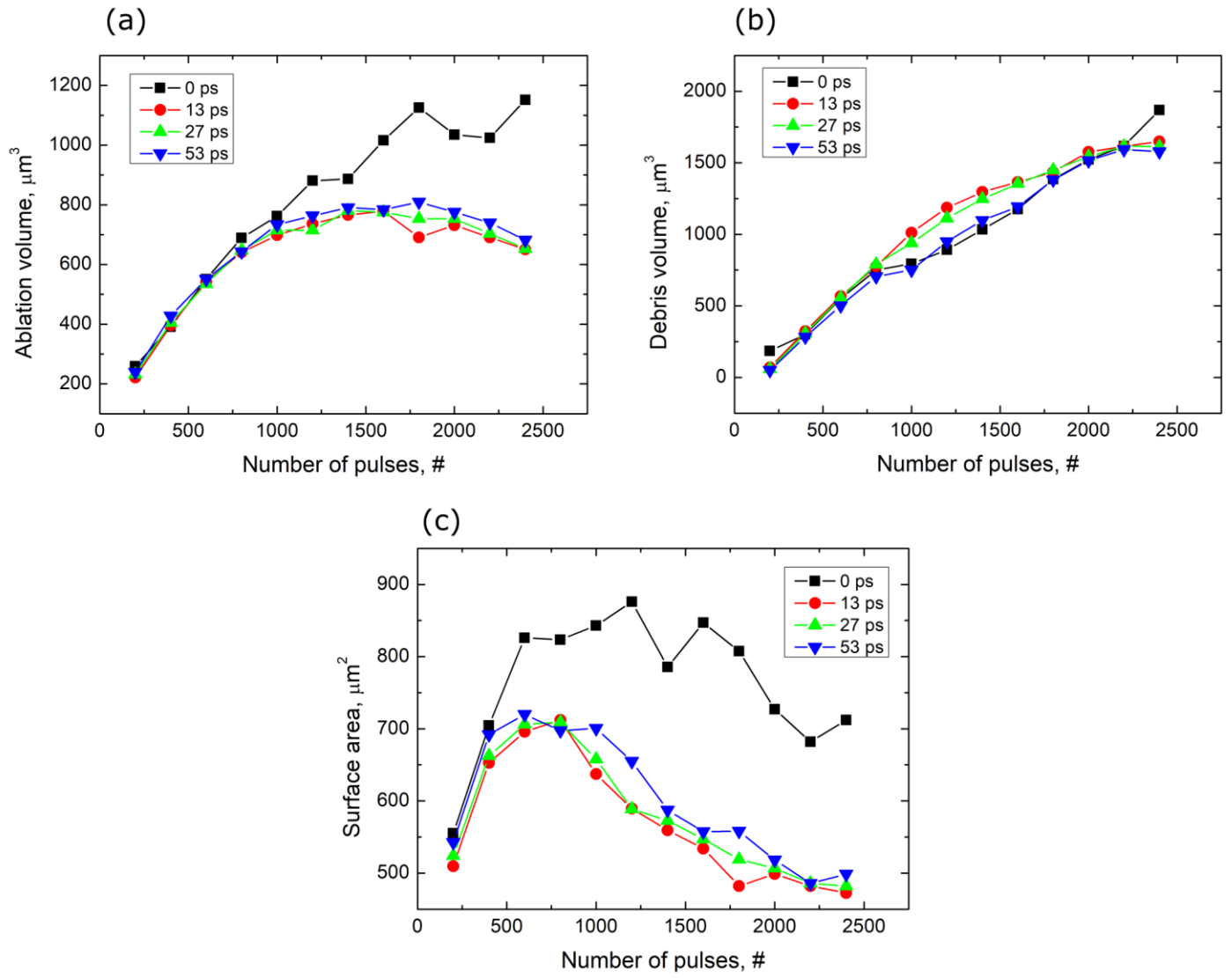

Fig. Ablation results based on delay between interfering pulses

Reduction in measured depth and volume

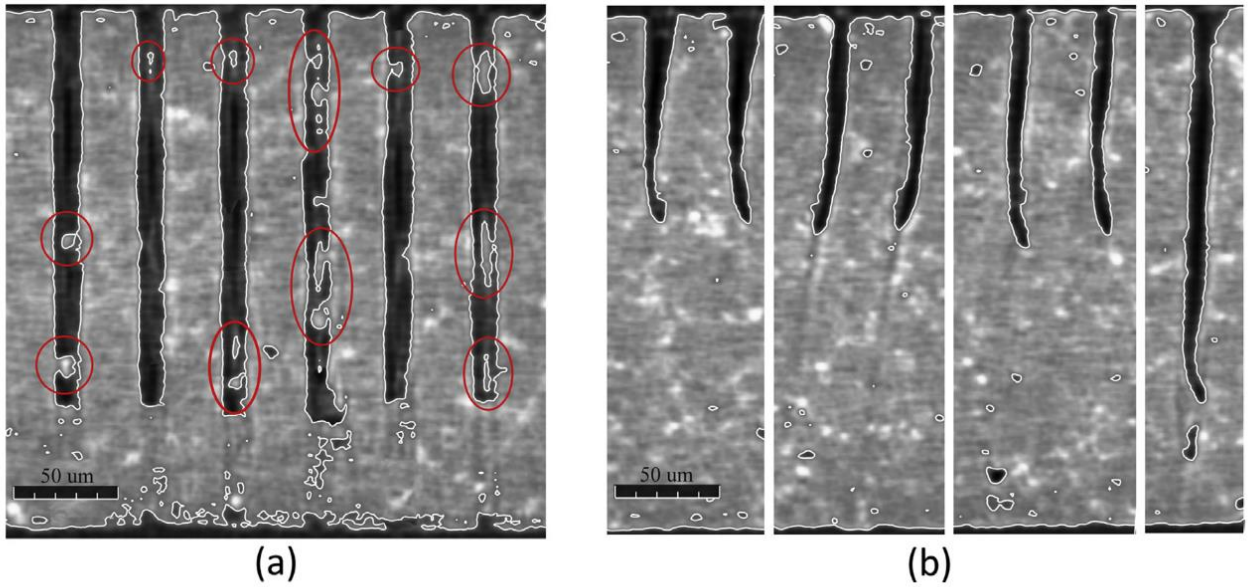

Fig. 8. Issues with high aspect ratio holes, (a) recasts and (b) bending. [1]

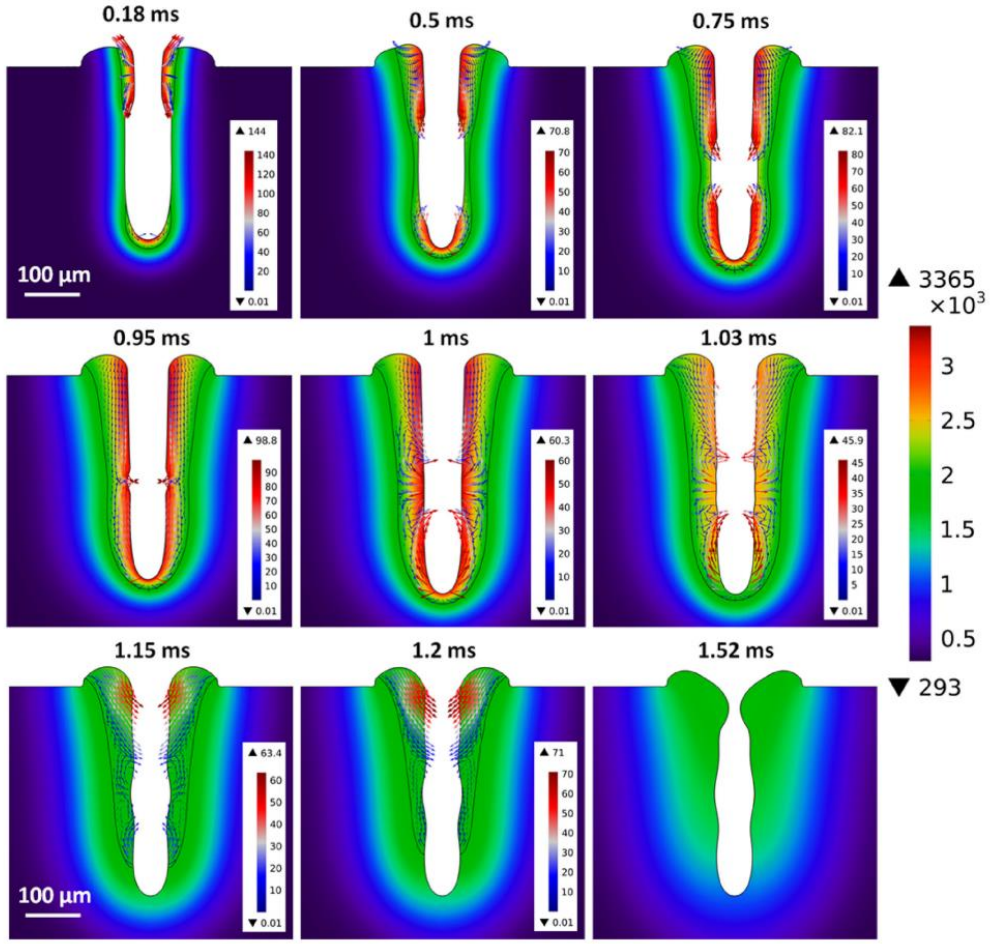

Fig. 12. Transient melt pool dynamics during the 8th pulse. Temperature field (color surface contour, unit: K), Velocity field (colored arrow plots, unit: mm/s). [2]

[1] V. Nasrollahi, Drilling of micro-scale high aspect ratio holes with ultra-short lasers (Doctoral dissertation, University of Birmingham), (2020)
[2] S. Sharma, et al., Journal of Materials Processing Technology **262**, (2018).


AČIŪ!

Laser Research Center

International Conference on Applied Physics & Imaging
(ICAPI)
20 - 21 September 2025 | Tartu, Estonia

Vilnius University
Excellence Center of Advanced Light Technologies

Generation of helical intensity beams and pulses for micromachining

Gabrielius Kontenis

Our group

Tartu, Estonia
2025-09-21